

Latent group structure and regularized regression

Konstantinos Perrakis¹, Frank Dondelinger² and Sach Mukherjee¹

¹*Statistics and Machine Learning,
German Center for Neurodegenerative Diseases (DZNE), Bonn, Germany.*

²*Lancaster Medical School, Lancaster University, UK.*

Abstract

Regression modelling typically assumes homogeneity of the conditional distribution of responses Y given features X . For inhomogeneous data, with latent groups having potentially different underlying distributions, the hidden group structure can be crucial for estimation and prediction, and standard regression models may be severely confounded. Worse, in the multivariate setting, the presence of such inhomogeneity can easily pass undetected. To allow for robust and interpretable regression modelling in the heterogeneous data setting we put forward a class of mixture models that couples together both the multivariate marginal on X and the conditional $Y|X$ to capture the latent group structure. This joint modelling approach allows for group-specific regression parameters, automatically controlling for the latent confounding that may otherwise pose difficulties, and offers a novel way to deal with suspected distributional shifts in the data. We show how the latent variable model can be regularized to provide scalable solutions with explicit sparsity. Estimation is handled via an expectation-maximization algorithm. We illustrate the key ideas via empirical examples.

Keywords: distribution shifts, heterogeneous data, latent group structure, mixture models, sparse regression

1 Introduction

Regression modelling assumes homogeneity of the conditional distribution of a response Y given features X in the sense that it is usually taken to be the case that the *same* conditional distribution holds for all samples. In the presence of latent groups that might have different underlying distributions, regression modelling may be severely confounded. This is a concern whenever data might harbour unrecognized distributional shifts, e.g. between data subsets that differ with respect to an unrecognized factor. In applied statistics and machine learning latent group structure is routinely dealt with via clustering, mixture models or related approaches. However – and as we argue in detail below – standard tools used for inhomogeneous data remain subject to limitations in modelling heterogeneity in multivariate regression. Motivated by this gap, in this paper we propose a class of mixture models in which both latent structure in the feature space and (potentially non-identical) group-specific regression models for the response are dealt with jointly. In loose (high-level) notation, we consider models of

the form

$$\begin{aligned} Z &\sim \pi_Z \\ X \mid Z=k &\sim p_X(\mu_k, \Sigma_k) \\ Y \mid X, Z=k &\sim p_Y(g(X\beta_k), \sigma_k^2) \end{aligned} \tag{1}$$

where Z is a latent indicator of group membership (taking values $k \in \{1, \dots, K\}$) with probability mass function π_Z , $p_W(m, s)$ denotes the probability density function of a continuous (univariate or multivariate) random variable W with location m and scale s , and $g(\cdot)$ a link function. This work focuses on the familiar and important case where both X and Y are normally distributed and g is the identity function. However, the key ideas apply to any model of the general form in (1).

In the setting under consideration the presence of group structure has the following consequences:

- *Confounding due to latent groups.* Associations between components of X and Y may be entirely different at the “global” level (with Z marginalized out) and at the “local” level (conditionally on Z). This applies also to the regression coefficients, with differences potentially even in signs (e.g. the global association might be positive and the local associations negative or *vice versa*) or sparsity patterns (a specific variable appearing in the true active set in one group but not in another). This is in effect a continuous, multivariate analogue to the classical Simpson’s paradox; see e.g. Pearl et al. (2016).
- *Ambiguous group structure in X -space.* Clustering the X ’s alone can give results that are unrelated to the setting or response of interest. This is due to the fact that many instances of genuine cluster signal in X (e.g. relatively high-density regions in the population distribution of X) may be unrelated to Y . For example, clustering gene expression data may yield clusters that while well-defined in the feature space may be unrelated to a specific biological or medical response of interest.
- *Group-specific signal in regression coefficients.* If indeed some coefficients are nonidentical across groups, then these coefficients provide a potentially useful discriminant signal for identifying the group structure itself. This signal is not contained in the distributions of the features (as it manifests only in the conditional distribution of the response) and therefore cannot be detected or exploited by simply clustering the X ’s.

Two common and simple strategies given paired data (X, Y) and a suspicion of latent group structure are:

- (S1) Ignore any potential grouping and fit one regression model using the entire data.
- (S2) Cluster the X ’s and then fit separate regression models to the group-specific data.

Neither strategy represents a principled solution as discussed in more detail in the next section. At this point it suffices to note the following. Strategy (S1) is particularly risky, since if latent group structure is present and the β_k ’s in (1) are non-identical, then the β ’s obtained via (S1) may be entirely incorrect. This is essentially a version of Simpson’s paradox (see Figure 1 below). Of course, whether or not such differences exist is unknown at the outset. We note also that under (S1) evaluation of predictive loss is not a satisfactory guide for model

assessment, since in some settings prediction error may be apparently small despite severe model misspecification. Strategy (S2) although safer is also not guaranteed to protect from Simpson’s type effects, unless the resulting group structure obtained from clustering the X ’s is correct with reference to the Y ’s; this may not hold in practical multivariate settings.

It is important to recognize that the Y ’s typically have a special status, representing something of specific interest in the problem setting. This motivates a need to exploit the information contained in the response variable to guide exploration of latent structure, since latent groups relevant to Y are in a sense particularly important. Importantly, the approach we propose allows for group-specific regression parameters which can safeguard against Simpson’s type effects. Moreover, as noted above, the group-specific coefficients may also provide a useful signal and serve to “focus” the clustering part of the problem on structure relevant to the response of interest.

The intersection of regression and latent variable modelling has been the topic of a rich body of previous work. A large and important class of methods relates to finite mixtures of regression (FMR) models, their numerous extensions (e.g. for generalized linear models and mixed models) and important variations (e.g. mixtures-of-experts models); see [McLachlan and Peel \(2000\)](#) and further [Khalili and Chen \(2007\)](#); [Städler et al. \(2010\)](#) for regularized FMR’s. Our approach is different from FMR modelling in the following sense. FMR models posit a mixture model for the conditional distribution of $Y | X$; this is quite different from our design as in this setting cluster allocation is solely focused on the relationship between Y and X , ignoring any discriminant source of signal from X (in a way FMR is the opposite of strategy S2). In multivariate problems this will be problematic unless part of the regression discriminant signal is extremely strong. Furthermore, by not modelling group structure in the X space, prediction of Y^* given a new X^* is not possible with FMR models as it is not feasible to allocate the newly observed feature point into a group. In contrast, this is possible in our design.

Another related latent modelling approach is profile regression ([Molitor et al., 2010](#); [Liverani et al., 2015](#)). Like our approach, profile regression jointly models X and Y . However, the corresponding graphical model under profile regression is different as X and Y are conditionally independent given the latent group indicator Z . In profile regression the effect of X on Y is essentially transferred and compacted to one “profile” parameter (a random intercept). Hence, the profile regression design does not support group-specific regression coefficients.

A relevant interesting work is also that of [Miller et al. \(2011\)](#) who extend product partition models (see e.g. [Crowley 1997](#)) to incorporate features. This framework is quite different than ours; here the effect of features (which are considered fixed) is incorporated in the probability of the partition set through the use of similarity functions. In principle, the proposed model can also include a regression link between Y and X (with group-specific coefficients); however, this case is not investigated in [Miller et al. \(2011\)](#).

In contrast, given input data of the form (X, Y) our approach estimates group structure and group-specific parameters jointly based on the hierarchical model specification presented in (1) coupled with regularization. [Ingrassia et al. \(2012\)](#) consider models of this form and is along the same lines as our work; however their work is limited to maximum-likelihood (ML) estimation. In the ML case the model in (1) (under the normal-normal setting with identity link, considered in this paper) is equivalent to a multivariate Gaussian mixture on (X, Y) ; see [Ingrassia et al. \(2012\)](#) for details. Under our approach, which couples the model in (1)

with regularization, the equivalence to the Gaussian mixture model no longer holds. We view regularization as fundamental to delivering a usable solution to this problem. In addition, in many cases p (number of features) may be on the same order as n (sample size), if not larger, and at the group level the sample sizes are strictly smaller. Furthermore, in our view it is precisely in large multivariate problems that the issues we allude to are most worrying, because the presence of group structure or distributional inhomogeneity can then easily pass undetected.

Regularization is used for those parts of the model in (1) where it is essential, in particular for the group-specific feature covariances and on the group-specific regression coefficients. In this work we utilize the graphical lasso (Meinshausen and Bühlmann, 2006; Friedman et al., 2008) for covariance estimation and consider two regularization approaches for the regression parameters: (i) the Bayesian version (Park and Casella, 2008) of lasso (Tibshirani, 1996) and (ii) regularization based on the normal-Jeffrey’s shrinkage prior (Figueiredo, 2001). We note that these choices are not fundamental for the proposed model specification and that in principle any other regularization method originating from the penalized least-squares or Bayesian shrinkage-prior literature could potentially be used. Lasso regularization is included because it is a well-established and recognized approach; the normal-Jeffrey’s approach is considered because as shown below it provides a tuning-free and easier-to-compute alternative within our expectation-maximization (EM) algorithm.

We note that in the present paper we focus on estimation given the number of groups. This focus is motivated by the fact that it is the model structure that is the main contribution of the present paper and there are many approaches for model order exploration or selection that could be applied in a model-based setting such as ours; see e.g. Celeux et al. (2018).

Henceforth, we will refer to our approach as *joint cluster regression* (JCR). In summary, the merits of JCR are the following:

- Combines information from X and from the regression of Y on X for cluster allocation;
- Yields group-specific regression coefficients with explicit sparsity patterns;
- Applicable in $p > n$ settings;
- Allows prediction of the response given a new feature vector X^* .

The remainder of the paper is structured as follows. Section 2 provides further motivation for the use of JCR, discussing a simple illustration which depicts particular cases of interest. In Section 3 we lay out the model specification, discuss the regularization methods under consideration and the correspondence between penalized likelihood and Bayesian solutions, and describe computationally efficient ways to set penalty parameters in the latent variable setting. Details of the EM and practical implementation of the algorithm are covered in Section 4. In Section 5 we discuss prediction using JCR and discuss how predictive measures can potentially be utilized for cluster selection when the number of groups is not predetermined. In Section 6 we present empirical examples, focusing initially on small – yet informative for illustrative purposes – problems and then proceeding to larger scale simulations based on real data. The paper concludes with a discussion in Section 7.

2 Illustration

Before describing the model and estimators in details, we consider a simple graphical illustration of the types of problems that JCR is designed to address. To allow for direct visualization, the illustration is for only one feature, but we emphasize that the goal in the sequel is to address multivariate analogues of the issues we describe in this section.

JCR is fully general in terms of differences in parameters between the hidden groups, but to fix ideas we consider three specific cases (multivariate generalizations of these cases appear in empirical work below). For ease of illustration assume that only one of the features X is influential (in the sense of having a non-zero, group-specific coefficient). Refer to this specific feature as x^* . The response is y and there are two latent groups with some separation between the group-wise means of x^* . Figure 1 shows the three cases: an equal-intercept/unequal-slope case (case A), a unequal-intercept/equal-slope case (case B) and an equal intercept and slope case (case C). Cases A and B have hidden differences in regression coefficients and are complicated to treat in the truly multivariate setting. In Case C, the problems of clustering and regression are clearly decoupled and therefore the two tasks may be performed independently (as long as group sample sizes are sufficiently large). However, since all model parameters are unknown at the outset, a classification of the problem into these and other cases cannot be easily done.

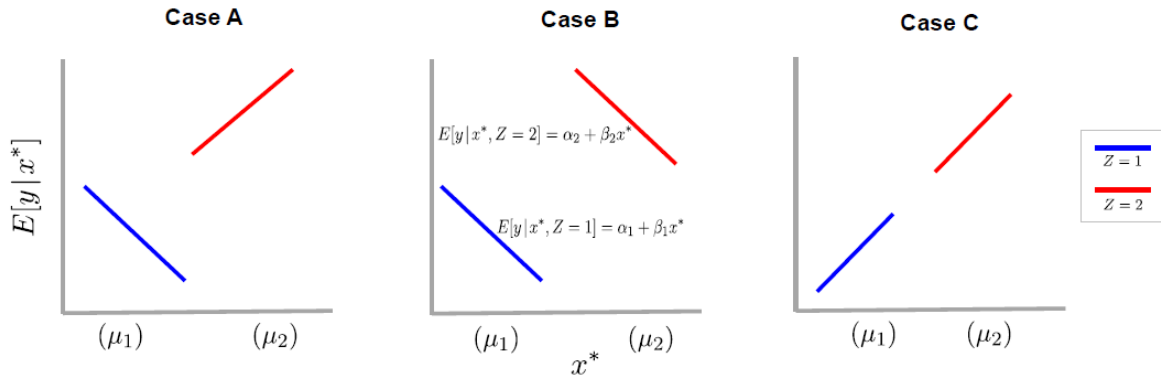


Figure 1: A univariate illustration of some interesting cases of group structure.

Case B illustrates the issues around interpretability mentioned above: under the strategy (S1), in which regression is simply carried out on the pooled data, the slope here may be *positive*, despite the group-specific slopes both being *negative*. Moreover, the prediction loss obtained in the pooled case may be small; e.g., in the particular example shown, the correlation between x^* and y grows larger as $|\mu_1 - \mu_2|$ grows. In the general multivariate setting, this kind of issue is difficult to detect or visualize and we refer to this as a multivariate, continuous generalization of Simpson’s paradox.

Clearly, any clustering tool or feature-space mixture model that does not include the group-specific signal from the regression part of the model will perform well only as long as the separation of the group-wise means is large enough. Furthermore, in multivariate settings there may exist many groupings in the feature space which are irrelevant to the specific response of interest. As discussed below and shown in the simulation examples of Section 6, JCR has the potential to effectively detect patterns such as those in Figure 1 and

to improve detection of latent group structure.

The plots provide some immediate intuition as to why joint estimation is of interest here. An important point is that while patterns like those in Figure 1 are obvious in one-dimensional toy examples, they are difficult to study and visualize in practical multivariate data analysis, where nevertheless such effects may be common (this is relevant also to issues around distributional shifts in prediction; see Section 7). Our intention is to put forward estimators that automatically address this kind of situation in the general multivariate case where direct visualization is difficult or impossible and where model parameters are unknown at the outset.

3 The JCR model

3.1 Model specification

Let \mathbf{y} denote an n -dimensional vector of responses and \mathbf{X} an $n \times p$ feature matrix. Samples are indexed by $i = 1, \dots, n$. Let K denote the number of groups and $z_i \in \{1 \dots K\}$ represent the true (latent) group indicator for the sample point (y_i, \mathbf{x}_i) with $\Pr(z_i = k) = \tau_k$. The group-specific parameters are $\boldsymbol{\theta}_k = (\boldsymbol{\theta}_k^X, \boldsymbol{\theta}_k^Y)^T$ with $\boldsymbol{\theta}_k^X$ and $\boldsymbol{\theta}_k^Y$ being the parameters governing respectively the marginal distribution of X and the regression model of Y on X .

We allow for group-specific parameters, but assume that samples are i.i.d. within groups. With the notation above, the joint sampling distribution of y_i and \mathbf{x}_i in group k is

$$p(y_i, \mathbf{x}_i | \boldsymbol{\theta}_k, z_i = k) = p(y_i | \boldsymbol{\theta}_k^Y, \mathbf{x}_i, z_i = k) p(\mathbf{x}_i | \boldsymbol{\theta}_k^X, z_i = k). \quad (2)$$

Our overall framework is general, but to fix ideas, and throughout the remainder of the paper, the features are modelled via p -dimensional multivariate normal distributions so that $\boldsymbol{\theta}_k^X = (\boldsymbol{\mu}_k, \text{vec}(\boldsymbol{\Sigma}_k))^T$, where $\boldsymbol{\mu}_k$ is the mean and $\boldsymbol{\Sigma}_k$ the $p \times p$ covariance matrix. For the responses, we specify a normal linear regression model, with parameters $\boldsymbol{\theta}_k^Y = (\alpha_k, \boldsymbol{\beta}_k, \sigma_k^2)^T$, where α_k is the intercept, $\boldsymbol{\beta}_k$ the vector of regression coefficients and σ_k^2 the error variance. Note that inclusion of the intercept is necessary in the present setting, because it is not possible to centre the response appropriately when the group labels are unknown.

Thus, we have that

$$p(\mathbf{x}_i | \boldsymbol{\theta}_k^X, z_i = k) \equiv p(\mathbf{x}_i | \boldsymbol{\mu}_k, \boldsymbol{\Sigma}_k, z_i = k) = \varphi_p(\mathbf{x}_i | \boldsymbol{\mu}_k, \boldsymbol{\Sigma}_k), \quad (3)$$

and

$$p(y_i | \boldsymbol{\theta}_k^Y, \mathbf{x}_i, z_i = k) \equiv p(y_i | \alpha_k, \boldsymbol{\beta}_k, \sigma_k^2, \mathbf{x}_i, z_i = k) = \varphi_1(y_i | \alpha_k + \mathbf{x}_i^T \boldsymbol{\beta}_k, \sigma_k^2), \quad (4)$$

where $\varphi_q(\cdot | \mathbf{m}, \boldsymbol{\Sigma})$ denotes the q -dimensional normal distribution with mean \mathbf{m} and variance-covariance $\boldsymbol{\Sigma}$. Marginalizing out the latent variables leads to a mixture representation of the form

$$p(\mathbf{y}, \mathbf{X} | \boldsymbol{\theta}, \boldsymbol{\tau}) = \prod_{i=1}^n \sum_{k=1}^K p(y_i | \boldsymbol{\theta}_k^Y, \mathbf{x}_i, z_i = k) p(\mathbf{x}_i | \boldsymbol{\theta}_k^X, z_i = k) \tau_k, \quad (5)$$

where $\boldsymbol{\theta} = (\boldsymbol{\theta}_1, \dots, \boldsymbol{\theta}_K)^T$ and $\boldsymbol{\tau} = (\tau_1, \dots, \tau_K)^T$. As discussed in Section 1 the model formulation arising from Eqs. (2) – (5) has been studied by Ingrassia et al. (2012) in the context of ML estimation. In that work the authors also show how the model in (5) includes as special cases finite mixtures of Gaussians (when applied to $\mathbf{W} \equiv [\mathbf{y}, \mathbf{X}]$), FMR's and mixtures-of-experts under certain conditions; for details see Ingrassia et al. (2012).

3.2 Regularization and priors

Given the likelihood function of $\boldsymbol{\theta}$ and $\boldsymbol{\tau}$ in (5) we consider general solutions of the form

$$\hat{\boldsymbol{\theta}}, \hat{\boldsymbol{\tau}} = \arg \max_{\boldsymbol{\theta}, \boldsymbol{\tau}} \left\{ \log p(\mathbf{y}, \mathbf{X} | \boldsymbol{\theta}, \boldsymbol{\tau}) + \sum_{k=1}^K \text{pen}(\boldsymbol{\theta}_k^{*X}) + \sum_{k=1}^K \text{pen}(\boldsymbol{\theta}_k^{*Y}) \right\}, \quad (6)$$

where $\text{pen}(\cdot)$ denotes a penalty function, and $\boldsymbol{\theta}_k^{*X}$ and $\boldsymbol{\theta}_k^{*Y}$ are parameter subsets (sub-vectors of $\boldsymbol{\theta}_k^X$ and $\boldsymbol{\theta}_k^Y$ respectively) that we wish to regularize.

The particular parameters we penalize are the group-specific covariances and the group-specific regression vectors. Hence, the penalized parameters in (6) are $\boldsymbol{\theta}_k^{*X} \equiv \text{vec}(\boldsymbol{\Sigma}_k)$ and $\boldsymbol{\theta}_k^{*Y} \equiv \boldsymbol{\beta}_k$ (although under one approach in Section 3.2.2 we consider $\boldsymbol{\theta}_k^{*Y} \equiv (\boldsymbol{\beta}_k, \sigma_k^2)^T$).

Penalization for these specific blocks of parameters is required because the corresponding ML estimates are either inefficient or ill-defined. Specifically, with respect to the covariances $\boldsymbol{\Sigma}_k$, ML estimates have a high variance when the number of predictors p is smaller than, but close to, the group-specific sample size n_k . Furthermore, in the $p > n_k$ case the sample covariance matrix (the ML estimate) is not positive definite and this also renders computation of the ML estimate of $\boldsymbol{\beta}_k$ intractable. In addition, sparsity patterns in $\boldsymbol{\beta}_k$ are of interest to shed light on important group-specific predictors.

We proceed with a detailed description of the specific penalty functions under consideration. We discuss our choices from both penalized likelihood and Bayesian viewpoints. The latter view is useful for three reasons. Firstly, due to the fact that the EM algorithm formulated in Section 4 essentially locates maximum a posteriori (MAP) estimates, as the penalties in (6) correspond to log-kernels of prior distributions. Secondly, because certain of our choices require starting with an explicit Bayesian formulation. Thirdly, because additional components, imposed by prior distributions on penalty tuning parameters and/or on the error variance σ_k^2 , will be added to the general solution in (6).

For the remainder of this Section it is easier to discuss the corresponding solutions under known group labels. In this case let us denote the $n_k \times 1$ response by \mathbf{y}_k and the $n_k \times p$ predictor matrix by \mathbf{X}_k for $k = 1, \dots, K$. The actual solutions under latent group labels are, of course, obtained iteratively via the EM algorithm presented in Section 4.

3.2.1 Regularization of $\boldsymbol{\Sigma}_k$

For the regularization of $\boldsymbol{\Sigma}_k$ we use the graphical lasso (Meinshausen and Bühlmann, 2006; Yuan and Lin, 2007; Friedman et al., 2008). The graphical lasso induces sparsity in the inverse covariance matrix, here denoted by $\boldsymbol{\Omega}_k = \boldsymbol{\Sigma}_k^{-1}$ for group k . Using the graphical lasso penalty we have that $\text{pen}(\boldsymbol{\theta}_k^{*X}) \equiv \text{pen}(\boldsymbol{\Omega}_k) = -\xi \|\boldsymbol{\Omega}_k\|_1$ in (6), where $\xi > 0$ controls the strength of regularization and $\|\cdot\|_q$ is the L_q norm. For known group labels the graphical lasso estimate would be given by

$$\hat{\boldsymbol{\Omega}}_k = \arg \max_{\boldsymbol{\Omega}_k \in M^+} \left\{ \log |\boldsymbol{\Omega}_k| - \text{tr}(\boldsymbol{\Omega}_k \hat{\mathbf{S}}_k) - \xi \|\boldsymbol{\Omega}_k\|_1 \right\}, \quad (7)$$

where M^+ is the space of positive definite matrices and $\hat{\mathbf{S}}_k$ is the ML covariance estimate of \mathbf{X}_k . As shown in Wang (2012) the solution in (7) is equivalent to the posterior mode under

a likelihood as in (3) and a prior distribution of the following form

$$p(\mathbf{\Omega}_k|\psi) \propto \left[\prod_{j=1}^p \text{Exp}(\omega_{kjj}|\psi/2) \prod_{j<l,l=2}^p \text{DE}(\omega_{kjl}|0, \psi^{-1}) \right] \mathbb{1}_{\{\mathbf{\Omega}_k \in M^+\}}, \quad (8)$$

where $\mathbb{1}_{\{\cdot\}}$ is the indicator function, $\text{Exp}(\cdot|r)$ is the exponential distribution with rate $r > 0$ and $\text{DE}(\cdot|\mu, b)$ is the double exponential (also referred to as Laplace or Gumbel) distribution with location $\mu \in \mathbb{R}$ and scale $b > 0$. The connection between the solution in (7) and the corresponding MAP estimate under the likelihood in (3) and the prior in (8) is that for any given value of ξ we have that $\psi = n_k \xi$. At this stage we encounter the first tuning parameter, ψ (or equivalently ξ) of the JCR model formulation.

As we will see throughout, tuning of such parameters is particularly difficult in the latent group setting. Two general strategies are as follows. The first one is to fix tuning parameters before initiating the EM. This would entail either using plug-in values (e.g. empirical Bayes estimates or “universal” thresholds from existing literature such as Donoho and Johnstone 1994; Städler and Mukherjee 2013) or searching over a grid of candidate values to optimize a specific criterion. The grid-search approach is computationally burdensome in the current setting, since an entire EM procedure would need to be considered at each grid point. The second strategy is to consider tuning parameters as free parameters under estimation. In this case, however, the only available criterion that will not affect the monotonicity of the EM algorithm is to maximize the objective function, which in turn makes sense only when tuning parameters are regulated via a prior distribution. This is straightforward to see in the case of the graphical lasso penalty, since maximizing (7) with respect to ξ in the absence of an additional prior log-kernel simply yields $\hat{\xi} = 0$. Thus, we advocate using either plug-in values or sensible prior distributions that facilitate estimation.

For the graphical lasso penalty, we use the “universal” threshold $\tilde{\psi} = \sqrt{2n \log p}/2$ derived from the logical arguments developed in Städler and Mukherjee (2013). Note that here we use n instead of n_k as the group labels will be unknown. The reason for choosing the universal-threshold approach for the graphical lasso is that we are less interested in the sparsity pattern of $\mathbf{\Omega}_k$ itself (studying which might indeed require a more careful fine-tuning of ψ). Rather, we mainly want a well-behaved estimate that allows group structure to be effectively revealed and studied. Indeed, provided group indicator estimation is sufficiently accurate the detailed sparsity patterns could be recovered in a final step, with fine-tuned penalization (doing so would require appropriate methods, such as data splitting to avoid bias, but we do not discuss this further here).

3.2.2 Regularization of β_k

For the group-specific vectors of regression coefficients we consider two regularization approaches. The first is based on the lasso (Tibshirani, 1996). The second, which comes from the Bayesian literature on shrinkage priors, is based on the normal-Jeffrey’s prior (Figueiredo, 2001). Both approaches provide simultaneous shrinkage and selection; we discuss each in turn.

The lasso approach. We consider a scaled version of the lasso, where the penalty in (6) is given by $\text{pen}(\boldsymbol{\theta}_k^{*Y}) \equiv \text{pen}(\boldsymbol{\beta}_k, \sigma_k^2) = \lambda_k \|\boldsymbol{\beta}_k\|_1 / \sigma_k$ with $\lambda_k > 0$. Note that here we introduce group specific penalty parameters λ_k , unlike previously, where parameter ψ is common across groups. This type of lasso regularization has been studied by Städler et al. (2010) in the

context of mixtures of regression models, a setting where the role of the scaling of variance parameters is much more important than in standard homogeneous regression, as remarked by the same authors.

If the groups were known, the lasso estimate would be

$$\hat{\alpha}_k, \hat{\boldsymbol{\beta}}_k, \hat{\sigma}_k^2 = \arg \min_{\alpha_k, \boldsymbol{\beta}_k, \sigma_k^2} \left\{ \frac{\|\mathbf{y}_k - \alpha_k \mathbf{1}_{n_k} - \mathbf{X}_k \boldsymbol{\beta}_k\|_2^2}{2\sigma_k^2} + \lambda_k \frac{\|\boldsymbol{\beta}_k\|_1}{\sigma_k} + (n_k + p + 2) \log \sigma_k \right\}, \quad (9)$$

where $\mathbf{1}_q$ denotes a q -dimensional vector of ones. Of course, for known group labels one could omit the intercept term and simply work with $\tilde{\mathbf{y}}_k = \mathbf{y}_k - \bar{y}_k \mathbf{1}_{n_k}$, but as we note above including these intercepts in the model is essential in the general hidden groups case. The solution in (9), which is slightly different than the one in Stadler et al. (2010), corresponds exactly to the posterior mode under the Bayesian lasso formulation (Park and Casella, 2008), that specifies independent double exponential priors for the regression coefficients conditional on the error variance which is assigned the scale-invariant Jeffrey’s prior. Namely,

$$p(\boldsymbol{\beta}_k | \sigma_k^2, \lambda_k) = \prod_{j=1}^p \frac{\lambda_k}{2\sigma_k} \exp\left(-\lambda_k \frac{|\beta_{kj}|}{\sigma_k}\right) \quad \text{and} \quad p(\sigma_k^2) \propto \frac{1}{\sigma_k^2}, \quad (10)$$

with the correspondence to (9) completed when $p(a_k) \propto 1$.

Tuning of the λ_k ’s for the regression component of JCR is more relevant from an inferential perspective than the tuning of the graphical lasso parameter ψ , as in this case we are directly interested in inferring about the sparsity patterns of the group regression vectors. To this end we propose two methods for handling λ_k ; one based on a data-dependent plug-in estimate which we call the fixed-penalty lasso (FLasso) and one based on the construction of a suitable prior which we refer to as random-penalty lasso (RLasso).

FLasso. This approach is essentially a two-step tuning procedure. We start with initial estimates, $\hat{\lambda}_k^{(0)}$ obtained via cross-validation (CV) based on some prior clustering of the data (this is needed in any case to initialize the EM). Then, at a certain EM iteration we recalculate the CV estimates and fix each group penalty to the new estimate $\hat{\lambda}_k^{(1)}$ for all further EM iterations. Specifically, we fix the parameter after the first iteration in which the group assignments (estimated group labels) do not change. From a Bayesian perspective the FLasso approach is essentially an empirical Bayes method as we use the data in order to plug-in $\hat{\lambda}_k^{(0)}$ and $\hat{\lambda}_k^{(1)}$ in the prior of $\boldsymbol{\beta}_k$ appearing in (10). The monotonic behaviour of the EM may be disrupted at the re-estimation iteration, but after that point it will hold. Also, the CV estimates can be easily calculated in the usual manner.

RLasso. For notational simplicity in the description of the RLasso approach we will temporarily omit the group indicator k . We propose placing a prior distribution on λ so that this parameter will be automatically updated during the EM (with the final estimate corresponding to the MAP value of λ). We want the prior to satisfy two requirements: (i) provide a lower and upper bound for λ , and (ii) support no penalization asymptotically ($\lambda \rightarrow 0$ as $n \rightarrow \infty$). The reasoning in having a lower as well as an upper bound is to avoid extremities in which the resulting solutions would be completely dense or sparse, respectively. The second requirement simply advocates the use of the ML estimates for the regression coefficients as $n \rightarrow \infty$. A suitable prior for our purposes is the truncated Pareto type-I distribution whose

scale parameter is also the lower bound of its support. The upper bound is set at one. The pdf of this distribution with scale $a_n > 0$ and shape $b_n > 0$ (the parameters are defined to depend on n) is given by

$$\pi(\lambda) = \frac{b_n a_n^{b_n}}{1 - a_n^{b_n}} \lambda^{-(b_n+1)} \quad \text{with } \lambda \in [a_n, 1]. \quad (11)$$

Under (11) the prior mode of λ is at a_n and the m -th moment is given by

$$E[\lambda^m] = a_n^m \frac{b_n}{b_n - m} \frac{1 - a_n^{b_n - m}}{1 - a_n^{b_n}} \quad (12)$$

for $b_n \neq 0$ and $m < b_n$. To satisfy the second prior requirement (no penalization asymptotically) we want $a_n \rightarrow 0$ and $b_n \rightarrow C$ as $n \rightarrow \infty$ (with constant $C > 2$ for the first and second moments to exist). We specify the shape hyper-parameter as follows

$$b_n = (p - 1) - c \sqrt{\frac{2 \log p}{n}}, \quad (13)$$

for some small positive c . Note that under (13) the first and second prior moments of λ exist as long as $p > c \sqrt{2 \log p / n} + 3$ (a realistic condition since we consider large p and small c). Furthermore, an explicit specification of a_n is not required as it does not affect the posterior mode of λ ; any decreasing function of n will satisfy our prior assumption. As shown next, specifying the prior via (11) and (13) will lead to a reasonable, interpretable update for λ during the M-step of the EM. Concerning constant c , empirical results indicated that values between 0.1 and 0.5 result in good performance. Under group notation we have λ_k and n_k throughout Eqs. (11) – (13).

The normal-Jeffrey’s approach. The normal-Jeffrey’s (NJ) prior (Figueiredo, 2001) consists of independent improper priors on the regression coefficients; in our context the prior is given by

$$p(\boldsymbol{\beta}_k) = \prod_{j=1}^p p(\beta_{kj}) \propto \prod_{j=1}^p |\beta_{kj}|^{-1}. \quad (14)$$

The corresponding penalized estimate induced by the NJ prior, under known group labels, is

$$\hat{\alpha}_k, \hat{\boldsymbol{\beta}}_k, \hat{\sigma}_k^2 = \arg \min_{\alpha_k, \boldsymbol{\beta}_k, \sigma_k^2} \left\{ \frac{\|\mathbf{y}_k - \alpha_k \mathbf{1}_{n_k} - \mathbf{X}_k \boldsymbol{\beta}_k\|_2^2}{2\sigma_k^2} + \sum_{j=1}^p \log |\beta_{kj}| + (n_k + 2) \log \sigma_k \right\}, \quad (15)$$

assuming again that $p(\alpha_k, \sigma_k^2) \propto 1/\sigma_k^2$. Here we have a penalty of the form $\text{pen}(\boldsymbol{\theta}_k^{*Y}) \equiv \text{pen}(\boldsymbol{\beta}_k) = \sum_{j=1}^p \log |\beta_{kj}|$.

The NJ prior is well known in the Bayesian literature related to shrinkage priors (Griffin and Brown, 2005; Carvalho et al., 2010; Polson and Scott, 2010). As is the case for most shrinkage priors, including the Bayesian lasso in (10), the prior in (14) can be expressed as a scale-mixture of normal distributions where for each β_{kj} we have that

$$p(\beta_{kj} | s_{kj}) = (2\pi s_{kj})^{-1/2} \exp(-\beta_{kj}^2 / 2s_{kj}) \quad (16)$$

with mixing distribution $\pi(s_{kj}) \propto s_{kj}^{-1}$, so that $\int p(\beta_{kj} | s_{kj}) \pi(s_{kj}) ds_{kj} \propto |\beta_{kj}|^{-1}$ for $j = 1, \dots, p$. Due to the fact that the mixing distribution lacks a further hyper-parameter the NJ prior

is characterized by the absence of a “global” scale parameter (penalty parameter from a penalized likelihood perspective). Also, due to the heavy tails of the NJ prior small coefficients are shrunk a lot, while large signals remain relatively unaffected; similarly to other heavy-tailed priors like the horseshoe (Carvalho et al., 2010) and the normal-exponential-gamma (Griffin and Brown, 2005). As shown in Figueiredo (2003) and Bae and Mallick (2004) the NJ prior strongly induces sparsity and yields good performance in terms of selection.

The use of the NJ prior is particularly appealing within the JCR framework for the following reasons. First, as discussed previously, tuning of penalty parameters is cumbersome in our setting and the available options (universal or empirical Bayes plug-ins, MAP estimates based on reasonable priors) require careful consideration. From this perspective, the NJ prior provides a much easier “tuning-free” alternative. As noted in Carvalho et al. (2010) shrinkage priors which lack a global scale parameter fail to capture the average signal density of the data; however, despite this potential shortcoming of the NJ prior the potential benefits are worth exploring. Second, as shown in Figueiredo (2003), the MAP estimate under the prior in (14) is easy to find through the use of an EM algorithm where the scaling parameters s_{kj} are considered latent. This additional latent structure can be easily incorporated in our EM framework without additional computational costs. In fact, the corresponding EM update is in closed-form, which is not the case in the lasso approach where we require a call to `glmnet`.

4 The JCR-EM algorithm

In this Section we present first the steps of the EM algorithm and proceed with a brief discussion of certain technical points. The EM algorithm for JCR includes maximization steps as well as conditional-maximization steps and is, therefore, a combination of the EM and the ECM (Meng and Rubin, 1993) algorithms. We present directly the corresponding objective functions and the parameter updates; for certain details that may not be immediately clear (under the NJ prior) we refer appropriately to Appendix A.

4.1 The EM steps

The E-Step. Irrespective of regularization approach, the group-membership probabilities of the mixture model in (5) at iteration t of the algorithm are calculated as

$$m_{ki}^{(t)} \equiv \widehat{\Pr}(z_i = k | y_i, \mathbf{x}_i, \boldsymbol{\theta}_k^{(t)}) = \frac{p(y_i | \boldsymbol{\theta}_k^{Y(t)}, \mathbf{x}_i, z_i = k) p(\mathbf{x}_i | \boldsymbol{\theta}_k^{X(t)}, z_i = k) \tau_k^{(t)}}{\sum_j p(y_i | \boldsymbol{\theta}_k^{Y(t)}, \mathbf{x}_i, z_i = k) p(\mathbf{x}_i | \boldsymbol{\theta}_k^{X(t)}, z_i = k) \tau_k^{(t)}}, \quad (17)$$

for $i = 1, \dots, n$, with the distributions appearing in the right-hand size of (17) defined in (3) and (4). We now define some quantities that will be used throughout; namely,

$$n_k^{(t)} = \sum_{i=1}^n m_{ki}^{(t)}, \quad \mathbf{m}_k^{(t)} = (m_{k1}^{(t)}, \dots, m_{kn}^{(t)})^T \text{ and } \mathbf{M}_k^{(t)} = \text{diag}(\mathbf{m}_k^{(t)}). \quad (18)$$

A convenient feature of the JCR design is that due to the hierarchical structure of the model the objective function can be split into separate simple parts. Specifically, we have that

$$Q(\boldsymbol{\theta}, \boldsymbol{\tau}, \boldsymbol{\lambda} | \boldsymbol{\theta}^{(t)}, \boldsymbol{\tau}^{(t)}, \boldsymbol{\lambda}^{(t)}) = Q^Y(\boldsymbol{\theta}^Y, \boldsymbol{\lambda} | \boldsymbol{\theta}^{Y(t)}, \boldsymbol{\lambda}^{(t)}) + Q^X(\boldsymbol{\theta}^X | \boldsymbol{\theta}^{X(t)}) + Q^Z(\boldsymbol{\tau} | \boldsymbol{\tau}^{(t)}), \quad (19)$$

where $\boldsymbol{\theta}^Y = (\boldsymbol{\theta}_1^Y, \dots, \boldsymbol{\theta}_K^Y)^T$ and $\boldsymbol{\theta}^X = (\boldsymbol{\theta}_1^X, \dots, \boldsymbol{\theta}_K^X)^T$. Here, by $\boldsymbol{\lambda}$ we denote the vector of group penalty parameters of the regression component of JCR. Depending upon regularization approach, the elements of vector $\boldsymbol{\lambda}$ at iteration t are fixed in the FLasso approach, free and under estimation in the RLasso approach, and absent in the NJ approach. Specifically,

$$\boldsymbol{\lambda}^{(t)} = \begin{cases} (\hat{\lambda}_1^{(t^*)}, \dots, \hat{\lambda}_K^{(t^*)})^T & \text{(FLasso),} \\ (\lambda_1^{(t)}, \dots, \lambda_K^{(t)})^T & \text{(RLasso),} \\ \emptyset & \text{(NJ),} \end{cases} \quad (20)$$

where $t^* = \{0, 1\}$ with zero and one corresponding to the initial CV estimate and the re-estimated CV value, respectively, of the penalty parameter under the FLasso approach discussed in Section 3.2.2.

Starting in reverse order from the right-hand side of (19) we have that

$$Q^Z(\boldsymbol{\tau}|\boldsymbol{\tau}^{(t)}) = \sum_{k=1}^K n_k^{(t)} \log \tau_k. \quad (21)$$

Following that, the second component of the objective function related to the parameters of the predictor matrix is given by

$$Q^X(\boldsymbol{\theta}^X|\boldsymbol{\theta}^{X(t)}) = \frac{1}{2} \sum_{k=1}^K \left[\sum_{i=1}^n m_{ki}^{(t)} \left[\log |\boldsymbol{\Omega}_k| - (\mathbf{x}_i - \boldsymbol{\mu}_k)^T \boldsymbol{\Omega}_k (\mathbf{x}_i - \boldsymbol{\mu}_k) \right] - \tilde{\psi} \|\boldsymbol{\Omega}_k\|_1 \right], \quad (22)$$

where $\tilde{\psi} = \sqrt{2n \log p}/2$ based on the rationale discussed in Section 3.2.1.

The last component Q^Y in (19) varies according to the regularization approach; therefore, we have to define two distinct functions, namely Q_{lasso}^Y and Q_{NJ}^Y . For the lasso approaches (FLasso/RLasso) we work with a re-parametrization of the form $\chi_k = \alpha_k/\sigma_k$, $\boldsymbol{\phi}_k = \boldsymbol{\beta}_k/\sigma_k$ and $\rho_k = \sigma_k^{-1}$, similarly to Stadler et al. (2010), in order to achieve convexity of the optimization problem. Specifically, we have that

$$Q_{\text{lasso}}^Y(\boldsymbol{\theta}^Y, \boldsymbol{\lambda}|\boldsymbol{\theta}^{Y(t)}, \boldsymbol{\lambda}^{(t)}) = \sum_{k=1}^K \left[- \frac{(\rho_k \mathbf{y} - \chi_k \mathbf{1}_n - \mathbf{X} \boldsymbol{\phi}_k)^T \mathbf{M}_k^{(t)} (\rho_k \mathbf{y} - \chi_k \mathbf{1}_n - \mathbf{X} \boldsymbol{\phi}_k)}{2} - \lambda_k \|\boldsymbol{\phi}_k\|_1 + (n_k^{(t)} + p + 2) \log \rho_k + f^{(t)}(\lambda_k) \right], \quad (23)$$

where

$$f^{(t)}(\lambda_k) = \begin{cases} 0 & \text{(FLasso),} \\ \sqrt{\frac{2 \log p}{n_k^{(t)}}} \log \lambda_k & \text{(RLasso).} \end{cases} \quad (24)$$

For the NJ approach the corresponding objective is given by

$$Q_{\text{NJ}}^Y(\boldsymbol{\theta}^Y|\boldsymbol{\theta}^{Y(t)}) = - \frac{1}{2} \sum_{k=1}^K \left[\frac{(\mathbf{y} - \alpha_k \mathbf{1}_n - \mathbf{X} \boldsymbol{\beta}_k)^T \mathbf{M}_k^{(t)} (\mathbf{y} - \alpha_k \mathbf{1}_n - \mathbf{X} \boldsymbol{\beta}_k)}{\sigma_k^2} + \boldsymbol{\beta}_k^T \mathbf{V}_k^{(t)} \boldsymbol{\beta}_k + (n_k^{(t)} + 2) \log \sigma_k^2 \right], \quad (25)$$

where

$$\mathbf{V}_k^{(t)} = \text{diag}\left(1/\beta_{k1}^{2(t)}, \dots, 1/\beta_{kp}^{2(t)}\right). \quad (26)$$

This diagonal matrix arises from the second underlying latent structure in the EM under the NJ prior, i.e. from the latent scale parameters in the hierarchical prior in (16). This method is introduced in Figueiredo (2003) for the normal linear regression model under the normal-Jeffrey's prior; further details are provided in Appendix A. As we will see below, matrix \mathbf{V}_k will in fact provide the final sparse estimate of β_k , as some of its diagonal entries gradually go to infinity during the EM; consequently, the diagonal entries of $\mathbf{U}_k = \mathbf{V}_k^{-1}$ that go to zero correspond to the coefficients that are set equal to zero.

The M-Step. From (21) we have that the group probabilities are updated as follows

$$\tau_k^{(t+1)} = \frac{n_k^{(t)}}{n}. \quad (27)$$

Concerning parameter block θ_k^x , from (22) we obtain the following updating equations

$$\boldsymbol{\mu}_k^{(t+1)} = \frac{\sum_{i=1}^n m_{ki}^{(t)} \mathbf{x}_i}{n_k^{(t)}} \quad (28)$$

and

$$\boldsymbol{\Omega}_k^{(t+1)} = \arg \max_{\boldsymbol{\Omega}_k} \left\{ \log |\boldsymbol{\Omega}_k| - \text{tr}(\boldsymbol{\Omega}_k \mathbf{S}_k^{(t)}) - \xi_k^{(t)} \|\boldsymbol{\Omega}_k\|_1 \right\}, \quad (29)$$

where in (29) we have that $\mathbf{S}_k^{(t)} = n_k^{-t} \sum_{i=1}^n m_{ki}^{(t)} (\mathbf{x}_i - \boldsymbol{\mu}_k^{(t+1)})(\mathbf{x}_i - \boldsymbol{\mu}_k^{(t+1)})^T$ and penalty parameter given by $\xi_k^{(t)} = \tilde{\psi}/n_k^{(t)} = \sqrt{2n \log p / (2n_k^{(t)})}$. Graphical lasso optimization is used to find the solution of (29); in practice we use the efficient R package `glassoFast` (Sustik and Calderhead, 2012).

For the lasso objective in (23) we have first the following updates for the group penalty parameters

$$\lambda_k^{(t+1)} = \begin{cases} \hat{\lambda}_k^{(t*)}, & \text{(FLasso update)} \\ \frac{c}{\|\boldsymbol{\phi}_k^{(t)}\|_1} \sqrt{\frac{2 \log p}{n_k^{(t)}}} = \frac{c}{\|\boldsymbol{\beta}_k^{(t)}\|_1} \left(\sigma_k^{(t)} \sqrt{\frac{2 \log p}{n_k^{(t)}}} \right) & \text{(RLasso update)}. \end{cases} \quad (30)$$

Note that the quantity inside the parenthesis in the second case of (30) is the optimal universal penalty under orthonormal predictors. The RLasso update is, therefore, a scaled version of the optimal penalty, with the scaling depending on the sparsity of the coefficients and on constant c . For the components of θ_k^y let us define first the quantities $\tilde{\mathbf{y}}_k^{(s)} = \mathbf{M}_k^{1/2(t)} (\mathbf{y} - \chi_k^{(s)} \mathbf{1}_n)$ and $\tilde{\mathbf{X}}_k^{(t)} = \mathbf{M}_k^{1/2(t)} \mathbf{X}$. The updates are then as follows

$$\rho_k^{(t+1)} = \frac{\sqrt{\left(\tilde{\mathbf{y}}_k^{(t)T} \tilde{\mathbf{X}}_k^{(t)} \boldsymbol{\phi}_k^{(t)}\right)^2 + 4(n_k^{(t)} + p + 2) \|\tilde{\mathbf{y}}_k^{(t)}\|_2^2 + \tilde{\mathbf{y}}_k^{(t)T} \tilde{\mathbf{X}}_k^{(t)} \boldsymbol{\phi}_k^{(t)}}}{2 \|\tilde{\mathbf{y}}_k^{(t)}\|_2^2}, \quad (31)$$

$$\chi_k^{(t+1)} = \frac{(\rho_k^{(t+1)} \mathbf{y} - \mathbf{X} \boldsymbol{\phi}_k^{(t)})^T \mathbf{m}_k^{(t)}}{n_k^{(t)}}, \quad (32)$$

$$\phi_k^{(t+1)} = \arg \min_{\phi_k} \frac{1}{2} \|\rho_k^{(t+1)} \tilde{\mathbf{y}}_k^{(t+1)} - \tilde{\mathbf{X}}_k^{(t)} \phi_k\|_2^2 + \lambda_k^{(t+1)} \|\phi_k\|_1. \quad (33)$$

In practice, for (33) we use a `glmnet` call with penalty equal to $\lambda_k^{(t+1)}/n_k^{(t)}$. Of course, the original parameters of interest are recovered at the last EM iteration via the inverse transformations $\alpha_k = \chi_k \sigma_k$, $\beta_k = \phi_k \sigma_k$ and $\sigma_k^2 = \rho_k^{-2}$.

Finally, the EM updates of θ_k^Y under the NJ prior are the following

$$\sigma_k^{2(t+1)} = \frac{(\mathbf{y} - \alpha_k^{(t)} \mathbf{1}_n - \mathbf{X} \beta_k^{(t)})^T \mathbf{M}_k^{(t)} (\mathbf{y} - \alpha_k^{(t)} \mathbf{1}_n - \mathbf{X} \beta_k^{(t)})}{n_k^{(t)} + 2}, \quad (34)$$

$$\alpha_k^{(t+1)} = \frac{(\mathbf{y} - \mathbf{X} \beta_k^{(t)})^T \mathbf{m}_k^{(t)}}{n_k^{(t)}}, \quad (35)$$

$$\beta_k^{(t+1)} = \left(\mathbf{X}^T \mathbf{M}_k^{(t)} \mathbf{X} + \sigma_k^{2(t+1)} \mathbf{V}_k^{(t)} \right)^{-1} \mathbf{X}^T \mathbf{M}_k^{(t)} (\mathbf{y} - \alpha_k^{(t+1)} \mathbf{1}_n). \quad (36)$$

As remarked previously, in practice we work with $\mathbf{U}_k^{(t)} = \mathbf{V}_k^{-1(t)}$ because elements of the latter matrix, given in (26), gradually go to infinity. Specifically, we have two available options for β_k ; the first is suited for the $n > p$ case and is given by

$$\beta_k^{(t+1)} = \mathbf{U}_k^{\frac{1}{2}(t)} \left(\sigma_k^{2(t+1)} \mathbf{I}_p + \mathbf{U}_k^{\frac{1}{2}(t)} \mathbf{X}^T \mathbf{M}_k^{(t)} \mathbf{X} \mathbf{U}_k^{\frac{1}{2}(t)} \right)^{-1} \mathbf{U}_k^{\frac{1}{2}(t)} \mathbf{X}^T \mathbf{M}_k^{(t)} (\mathbf{y} - \alpha_k^{(t+1)} \mathbf{1}_n), \quad (37)$$

while the second which is given by

$$\begin{aligned} \beta_k^{(t+1)} &= \sigma_k^{-2(t+1)} \mathbf{U}_k^{(t)} \left[\mathbf{I}_p - \mathbf{X}^T \left(\sigma_k^{2(t+1)} \mathbf{M}_k^{-1(t)} + \mathbf{X} \mathbf{U}_k^{(t)} \mathbf{X}^T \right)^{-1} \mathbf{X} \mathbf{U}_k^{(t)} \right] \\ &\quad \times \mathbf{X}^T \mathbf{M}_k^{(t)} (\mathbf{y} - \alpha_k^{(t+1)} \mathbf{1}_n) \end{aligned} \quad (38)$$

is faster to compute when $n < p$.

4.2 Practical implementation

We initialize the algorithm via a simple clustering of the data. For this we use R package `mclust`. Through the resulting group assignments we obtain initial estimates $\theta_k^{X(0)}$ and $\theta_k^{Y(0)}$. In order to initiate EMs from different starting points we add random perturbations to $\mu_k^{(0)}$, $\beta_k^{(0)}$ and $\sigma_k^{2(0)}$ and positive random perturbations to the diagonal elements of $\Sigma_k^{(0)}$. The multiple EMs can be easily run in parallel. As a default option we use ten EM starts.

For the termination of the algorithm we use a combination of two criteria that are commonly used in practice. The first is to simply set a maximum number (T) of EM iterations. Empirical results suggest that the option $T = 20$ is sufficient. The second criterion takes into account the relative change in the objective function in (19); namely, the algorithm is stopped when

$$\left| \frac{Q(\theta, \tau, \lambda | \theta^{(t)}, \tau^{(t)}, \lambda^{(t)})}{Q(\theta, \tau, \lambda | \theta^{(t-1)}, \tau^{(t-1)}, \lambda^{(t-1)})} - 1 \right| \leq \epsilon \quad (39)$$

using as default option $\epsilon = 10^{-6}$. Moreover, the algorithm is stopped, and results are discarded, when the sample size of a certain group becomes prohibitively small for estimation.

We define this criterion as a function of total sample size and the number of groups. Specifically, we terminate if $\min_k n_k^{(t)} \leq n/(10K)$.

As a final remark, we must note that because the graphical lasso and lasso solutions in (29) and (33), respectively, are not exact, monotonicity of the EM is in general not guaranteed. However, in practice we find that the behaviour of the algorithm is quite stable.

5 Prediction and cluster selection

An interesting feature of JCR, which is not available under mixtures of regression models, relates to prediction. Specifically, given a new observation $\mathbf{x}^* = (x_1^*, x_2^*, \dots, x_p^*)^T$ we can infer the cluster allocation of this observation via the quantities

$$\hat{\pi}_k^* \propto \hat{\tau}_k \varphi_p(\mathbf{x}^* | \hat{\boldsymbol{\mu}}_k, \hat{\boldsymbol{\Sigma}}_k), \quad (40)$$

where $\hat{\tau}_k$, $\hat{\boldsymbol{\mu}}_k$ and $\hat{\boldsymbol{\Sigma}}_k$ are EM estimates for $k = 1, \dots, K$. Predicting the value of y^* is then straightforward using the simple estimate

$$\hat{y}^* = \hat{\alpha}_{\tilde{k}} + \mathbf{x}^{*T} \hat{\boldsymbol{\beta}}_{\tilde{k}}, \quad \text{with } \tilde{k} = \arg \max_k \hat{\pi}_k \quad (41)$$

where again $\hat{\alpha}_{\tilde{k}}$ and $\hat{\boldsymbol{\beta}}_{\tilde{k}}$ are the corresponding estimates from the EM. This predictive approach could be used as an inferential tool in the setting where the number of latent groups is not known *a priori*. This setting is, of course, not our primary focus in this paper. However, the idea of determining the number of clusters based on predictive loss is generally interesting as it connects supervised and unsupervised learning and has connections also to learning under distribution shifts (see Section 7 and the references therein) and, we therefore briefly discuss it here. We also present some first results in the simulation study of Section 6.2.2.

Specifically, the proposal is to select the number of clusters by first defining a sensible grid over K (depending on sample size) and then finding the model which minimizes predictive loss with respect to the response vector. Naturally, this will entail data splitting into training and testing samples, which can be a drawback, especially in the small sample setting. On the other hand, this approach provides a simple and quite natural way of determining the number of clusters based on a “guided” search that aims to optimize prediction of \mathbf{y} (which is the main variable of interest), taking account of group-specific predictive models.

In more detail, we aim to minimize the average group-wise predictive loss under the L_2 norm across competing models with a different number of clusters. Let \mathcal{G} denote the set of the number of clusters under consideration, so that the cluster indicator under model $g \in \mathcal{G}$ is $k_g = 1, \dots, K_g$. Following the rationale outlined above in Eqs. (40) and (41), under each model g we can obtain cluster allocations for a subset of held-out test data \mathbf{y}^* and \mathbf{X}^* . Denote by $\mathbf{y}_{k_g}^*$ the $n_{k_g}^* \times 1$ test-response vector and by $\mathbf{X}_{k_g}^*$ the $n_{k_g}^* \times p$ test-feature matrix assigned to group $k_g = 1, \dots, K_g$ conditional on g . Then, the solution for the “best” group-wise predictive model is given by

$$\hat{g} = \arg \min_{g \in \mathcal{G}} \left\{ \frac{1}{K_g} \sum_{k_g=1}^{K_g} \frac{\|\mathbf{y}_{k_g}^* - \hat{\alpha}_{k_g} \mathbf{1}_{n_{k_g}^*} - \mathbf{X}_{k_g}^{*T} \hat{\boldsymbol{\beta}}_{k_g}\|_2^2}{n_{k_g}^*} \right\}. \quad (42)$$

We note in passing that the same predictive approach for model selection could in principle be used for multivariate Gaussian mixtures when applied jointly to the response variable and

the feature matrix, as the marginal of \mathbf{X} and the conditional $\mathbf{y}|\mathbf{X}$ are known. Of course, as discussed in the Introduction, this model is not equivalent to JCR, so the resulting solutions will be different.

6 Empirical examples

In this Section we present two simulation examples which are based on the three specific cases summarized in Figure 1. Section 6.1 covers a small-scale (with respect to p) simulation which allows us to evaluate and visualize easily the various inferential aspects of the proposed modelling approach. In Section 6.2 we utilize real feature matrices in two semi-synthetic examples of realistically large scale. For JCR-RLasso the constant in (13) is set equal to 0.25.

6.1 A small-scale simulation

Set-up. We consider two groups ($K = 2$) with total $n = 100$ and balanced group sample sizes, i.e. $n_k = 50$ for $k = 1, 2$. The number of predictors is $p = 10$. In each group only the first predictor (\mathbf{x}_{k1}) has a non-zero effect on the response, i.e. only $\beta_{k1} \neq 0$ for $k = 1, 2$. The covariates are generated as $\mathbf{X}_k \sim N_p(\boldsymbol{\mu}_k, \boldsymbol{\Sigma}_k)$, with $\boldsymbol{\mu}_1 = (0, \dots, 0)^T$ and $\boldsymbol{\mu}_2 = (1, \dots, 1)^T$ being of dimensionality $p \times 1$. Thus, we assume different group-wise predictor means as in Figure 1. For the covariances we consider two scenarios. Firstly, an *uncorrelated-scenario* with diagonal covariances of the form $\boldsymbol{\Sigma}_1 = \boldsymbol{\Sigma}_2 = \mathbf{I}_p$. Secondly, a *correlated-scenario* with non-diagonal covariances, where each variable \mathbf{x}_{kj} , for $j = 2, \dots, p$, is again Gaussian noise, but the signal variable \mathbf{x}_{k1} is generated as

$$\mathbf{x}_{k1} \sim N_{n_k}(1.5\mathbf{x}_{k3} + 0.5\mathbf{x}_{k5} - 0.7\mathbf{x}_{k7}, 0.5\mathbf{I}_{n_k}),$$

for $k = 1, 2$. The response variable for each group is generated as

$$\mathbf{y}_k \sim N_{n_k}(\mathbf{1}_{n_k}\alpha_k + \mathbf{x}_{k1}\beta_{k1}, \sigma_k^2\mathbf{I}_{n_k}).$$

Specification of the slopes and intercepts is along the lines of the three cases covered in Figure 1; the specific values we use are summarized in Table 1. Finally, the error variance σ_k^2 of each group is set so that the correlation between test data (for test group sample sizes of 250) and predictions from a lasso model (using 10-fold cross-validation for tuning the penalty) is approximately 0.8 when group labels are known. The results that follow are from 50 repetitions of each simulation. We focus on regression signal detection, estimation of slope coefficients and group assignment performance.

Signal detection. The variable inclusion frequencies (over the 50 repetitions) for the uncorrelated scenario are presented in Figure 2. JCR-NJ performs better overall as it detects the influential effects all or almost all of the times and results in inclusion rates which are much lower than 50% for the non-influential effects. JCR-FLasso is effective in detecting the signals but produces much denser solutions as it frequently includes irrelevant variables. Interestingly, JCR-RLasso solutions are sparser in comparison to FLasso but not as sparse as the JCR-NJ solutions. Also, RLasso seems less effective in signal detection. The variable inclusion frequencies for the correlated scenario are shown in Appendix B (Figure B.1).

Case	Group	Intercept	Slope
A	1	0	1
	2	0	-1
B	1	0	1
	2	1	1
C	1	0	1
	2	0	1

Table 1: First simulation. Intercept and slope parameter values for the two groups under the three cases illustrated in Figure 1.

Overall, we would expect the noise variables which are correlated with the signal variables to have higher inclusion frequencies. However, except of some particular cases (under the Lasso approaches), the inclusion frequencies are in general very similar to those presented in Figure 2.

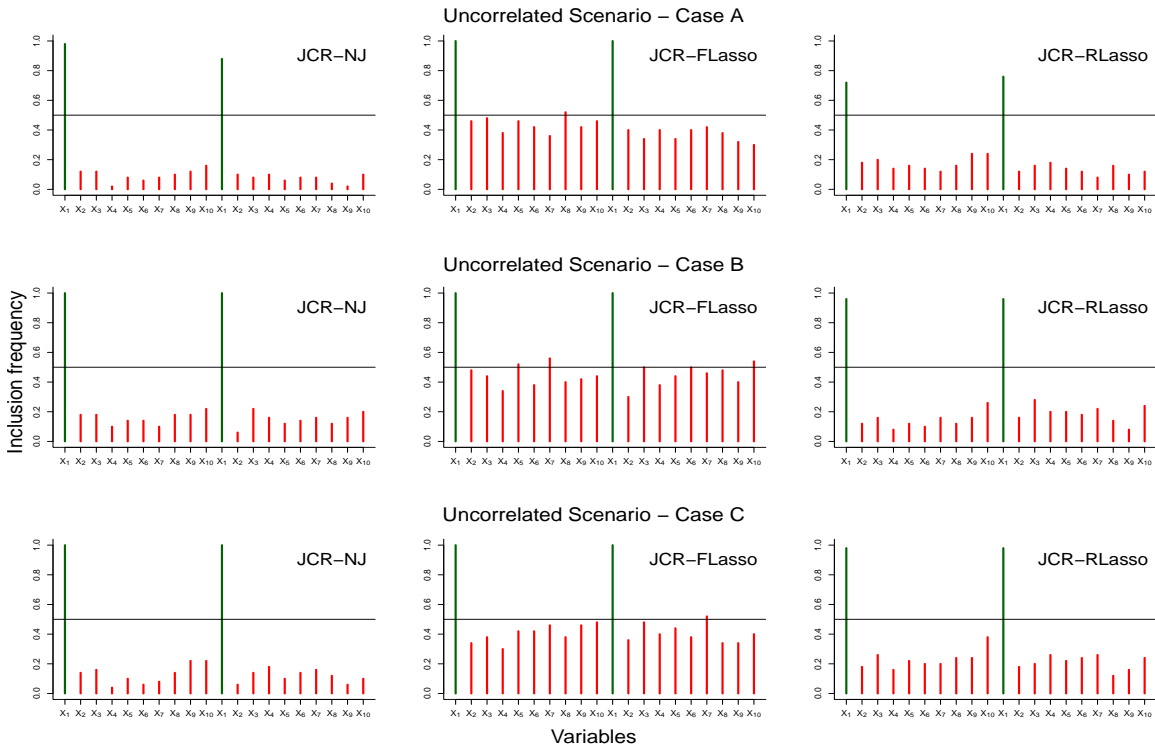


Figure 2: First simulation, uncorrelated scenario. Variable inclusion frequencies (under 50 repetitions) for signal variables (members of the true active set; in green) and non-signal variables (in red) for regression cases A, B and C. Horizontal black lines correspond to a frequency of 0.5.

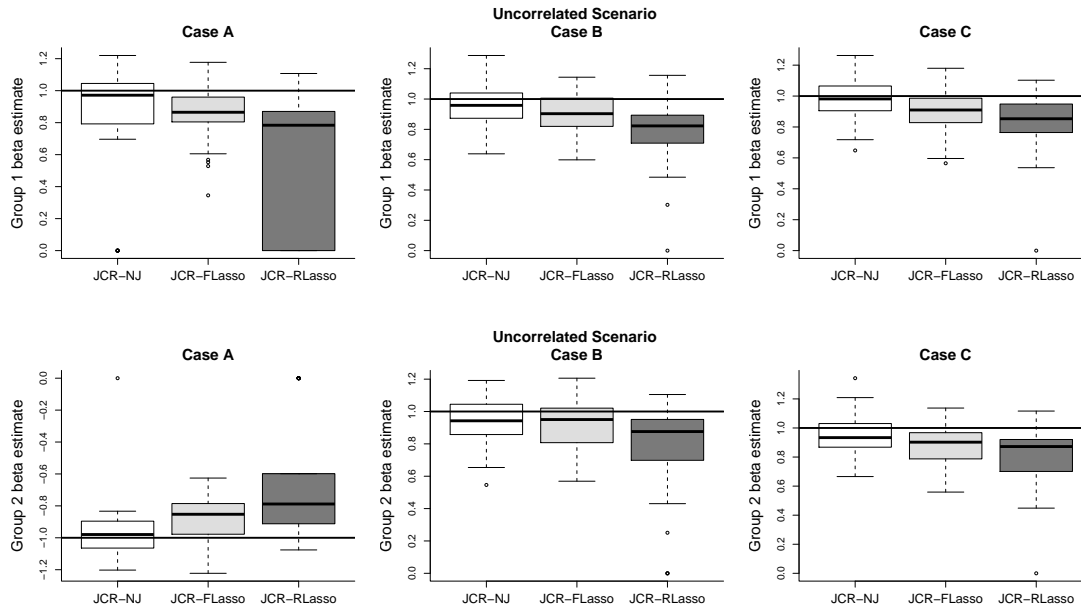


Figure 3: First simulation, uncorrelated scenario. Boxplots of slope estimates (from 50 repetitions) of all JCR methods for regression cases A, B and C. Horizontal black lines correspond to the true, data-generating slopes.

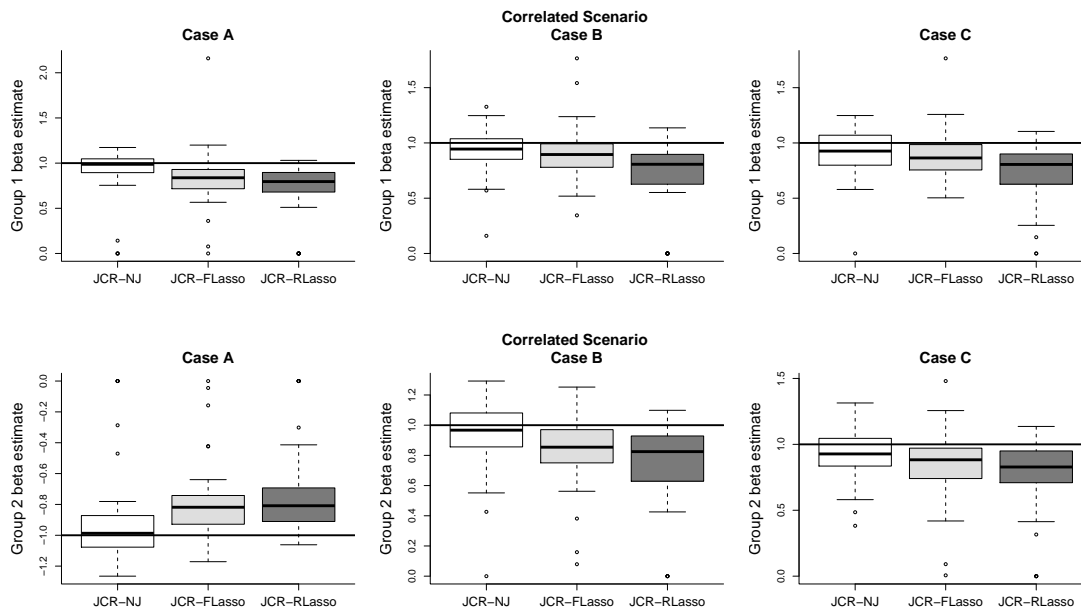


Figure 4: First simulation, correlated scenario. Boxplots of slope estimates (from 50 repetitions) of all JCR methods for regression cases A, B and C. Horizontal black lines correspond to the true, data-generating slopes.

Estimation of slope. Boxplots of slope estimates for the three regression cases are presented in Figure 3 (uncorrelated scenario) and Figure 4 (correlated scenario). As seen the estimates obtained from JCR-NJ are overall more accurate than the FLasso and RLasso estimates. Also, the RLasso group 1 slope estimate has large variability in the uncorrelated scenario under case A. The corresponding plots for the intercept terms are presented in Appendix B (Figures B.2 and B.3). In general, conclusions are the same; all three methods yield estimates close to the true intercepts, but the NJ estimates are slightly more accurate.

Latent group assignment. For the evaluation of assignment of the samples to latent groups we consider the adjusted Rand index between the actual (true) labels and the estimated labels resulting from the three JCR methods under consideration. Boxplots are presented in Appendix B (Figure B.4); group assignment performance is more or less the same across methods. We also notice that the performance tends to become worse as we shift from case A to case C. This is to be expected because case C has no discriminating signal in the regression component and has in that sense a strictly lower signal strength with respect to the assignment problem.

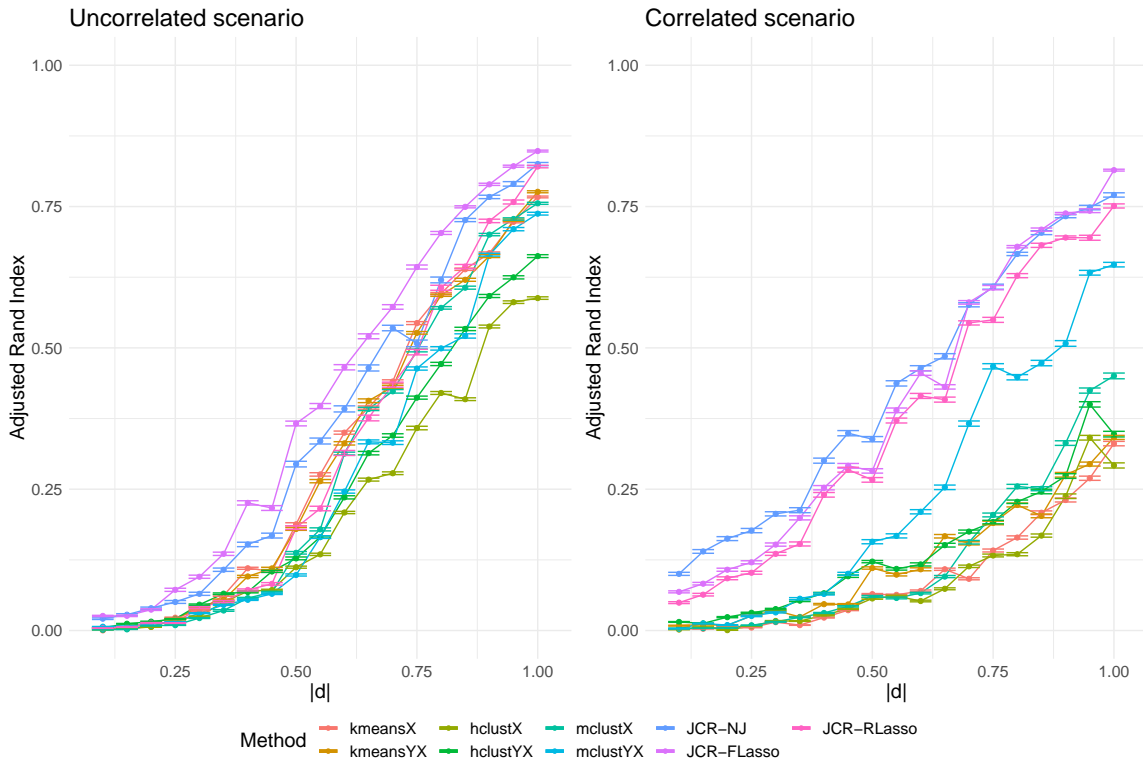


Figure 5: First simulation, case A. One standard-error plots of adjusted Rand index averages (from 50 repetitions) vs absolute distance ($|d|$) of the group-wise covariate means under the uncorrelated scenario (left) and correlated scenario (right).

A natural question is whether including the regression part of the model within a unified framework provides any empirical gains with respect to simply clustering the X matrix. In practice, between-group differences in means may be subtle, hence we consider in particular performance as the magnitude of the mean difference varies. In the foregoing results we used

$\boldsymbol{\mu}_1 = \mathbf{0}_p$ and $\boldsymbol{\mu}_2 = \mathbf{1}_p$. Now, we consider $\boldsymbol{\mu}_2 = \mathbf{0}_p + d\mathbf{1}_p$ with scalar $d = h \cdot u$, where h defines a grid ranging from 0.1 to 1 with a step of 0.05 and u is a random (uniform) sign. That is, $|d|$ is a measure of the strength of the mean signal. The methods we compare with are K -means, hierarchical clustering and mixture modelling (as implemented in R using the default options of `kmeans`, `hclust` and `Mclust` respectively; for the latter the BIC-best model is used). In addition, for each approach we use as input: (i) only \mathbf{X} and (ii) \mathbf{X} together with \mathbf{y} stacked in one data matrix. The latter represents an *ad hoc* approach to including the signal from the responses.

One standard-error plots of the resulting adjusted Rand index averages (from the 50 repetitions) as functions of $|d|$ are presented in Figure 5 for case A. As seen, JCR approaches can significantly improve group assignment results. The corresponding plots for cases B and C are presented in Appendix B; Figures B.5 and B.6, respectively. Even in these cases (where JCR is over-parameterized) our methods remain competitive in the uncorrelated scenario, while lead to better overall group assignment in the correlated scenario. In the latter case, distance-based methods perform poorly in general.

6.2 Semi-synthetic example based on real cancer data

The simulations presented below are based on real data from the The Cancer Genome Atlas (TCGA, <https://cancergenome.nih.gov>), a large-scale study of patient samples in cancer. Here we specifically use a data subset which was previously utilized in Taschler et al. (2019); see therein for details on data processing. Our rationale is to anchor the simulation in real covariance structures (Taschler et al., 2019). The data consist of gene expression values from four cancer types; breast (BRCA), kidney renal clear cell (KIRC), lung adenocarcinoma (LUAD) and thyroid (THCA). Our general strategy is to treat the cancer type as hidden: this allows us to test our approaches against differential covariance structure as seen in a real group-structured problem whilst having access to the true labels against which group assignments can be objectively tested. In the simulation of Section 6.2.1 we utilize covariates from the BRCA and KIRC data sources (i.e. $K = 2$) and compare to other methods with a focus on latent group identification, variable selection and estimation performance. In Section 6.2.2 we consider all four cancer types and provide some results on cluster selection under unknown number of groups.

6.2.1 Inference under two known groups

Set-up. For all simulations we consider $n = 250$, balanced group sample sizes, i.e. $n_k = 125$ for $k = 1, 2$, and varying dimensionality for the covariates; namely, i) $p = 100$ ($n > p$ problem), ii) $p = 250$ ($n = p$ problem) and iii) $p = 500$ ($n < p$ problem). We consider sparse problems where the percentage of non-zero regression coefficients ($\boldsymbol{\beta}^*$) is $s = 4\%$.

We consider the (arguably realistic) setting in which some of the non-zero coefficients are at common locations and others are at disjoint locations across the two groups (specifically, we place half the non-zero coefficients at common locations). As we will see, specification of the common-location $\boldsymbol{\beta}_k^*$'s will determine the three general cases depicted initially in Figure 1. Also, as we focus on sparse settings we do not want to allow the non-zero coefficients to take small values within the interval $(-0.1, 0.1)$. To this end let us denote the truncated normal distribution as $\text{TN}(\mu, \sigma^2, l, u)$ where as usual $\mu \in \mathbb{R}$, $\sigma^2 \geq 0$ and l, u are the respective

lower and upper truncation bounds. Let also $\text{mTN}(\mu, \sigma^2, a, b)$ denote the specific mixture of $\text{TN}(\mu, \sigma^2, -\infty, a)$ and $\text{TN}(\mu, \sigma^2, b, \infty)$ with $a < b$ and mixing parameter equal to 0.5; essentially, a truncated normal with support everywhere except the interval (a, b) . Group specific intercept values and slope-generating mechanisms, based on the three cases of Figure 1, are summarized in Table 2 (the setting of $\tilde{\sigma}^2$ is discussed just below). Given the matrices \mathbf{X}_k , the intercepts α_k and the sparse vectors β_k the response is generated as follows $\mathbf{y}_k \sim N_{n_k}(\mathbf{m}_k, \mathbf{I}_{n_k}\sigma_y^2)$, where $\mathbf{m}_k = \mathbf{I}_{n_k}\alpha_k + \mathbf{X}_k\beta_k$ for $k = 1, 2$ and $\sigma_y^2 = 1$. The scale parameter $\tilde{\sigma}^2$ in Table 2 is tuned so that the overall signal-to-noise under each case is approximately equal to three; i.e. $\text{Var}(\mathbf{m})/\sigma_y^2 \approx 3$ and $\mathbf{m} = (\mathbf{m}_1, \mathbf{m}_2)^T$.

Case	Group	Intercept	Slopes	
			Common locations	Disjoint locations
A	1	$\alpha_1 = \alpha_2 = 0$	$\beta_1^* \sim \text{TN}(0, \tilde{\sigma}^2, -\infty, -0.1)$	$\beta_1^* \sim \text{mTN}(0, \tilde{\sigma}^2, -0.1, 0.1)$
	2		$\beta_2^* \sim \text{TN}(0, \tilde{\sigma}^2, 0.1, \infty)$	$\beta_2^* \sim \text{mTN}(0, \tilde{\sigma}^2, -0.1, 0.1)$
B	1	$\alpha_1 = 0$	$\beta_1^* = \beta_2^* \sim \text{mTN}(0, \tilde{\sigma}^2, -0.1, 0.1)$	$\beta_1^* \sim \text{mTN}(0, \tilde{\sigma}^2, -0.1, 0.1)$
	2	$\alpha_2 = 1$		$\beta_2^* \sim \text{mTN}(0, \tilde{\sigma}^2, -0.1, 0.1)$
C	1	$\alpha_1 = \alpha_2 = 0$	$\beta_1^* = \beta_2^* \sim \text{mTN}(0, \tilde{\sigma}^2, -0.1, 0.1)$	$\beta_1^* \sim \text{mTN}(0, \tilde{\sigma}^2, -0.1, 0.1)$
	2			$\beta_2^* \sim \text{mTN}(0, \tilde{\sigma}^2, -0.1, 0.1)$

Table 2: Second simulation. Intercept values and slope-generating mechanisms for the two groups under the three cases illustrated in Figure 1.

We consider performance as a function of the absolute distance $|d|$ between the group-wise covariate means $\boldsymbol{\mu}_1$ and $\boldsymbol{\mu}_2$. We initially normalize the feature matrices, so that $\boldsymbol{\mu}_1 = \boldsymbol{\mu}_2 = \mathbf{0}$, and consider again the case where each element of $\boldsymbol{\mu}_2$ is shifted by $d = h \cdot u$, where $h \in \{0.1, 0.2, 0.4, 0.5, 0.6, 0.8, 0.9\}$ defines the grid and u is as previously a random uniform sign. Each simulation is repeated 20 times using random subsamples of covariate matrices from the original data. Here we present results for the $n < p$ setting ($n = 250, p = 500$); the corresponding results for $p = \{100, 250\}$ can be found in Appendix C.

For the regression questions addressed below our aim is to compare JCR with the simple “clustering-then-regression” approach. Obviously, a range of regression methods could be utilized in the second step. Since the simulations are sparse and linear by design, we will focus on lasso regression.

Group assignment. We start by an assessment of cluster allocation, comparing our approaches to the same competing methods considered in Section 6.1. Figure 6 presents error plots of the resulting adjusted Rand index averages over the grid of $|d|$. In general, we observe a phase-transition type of behaviour as all methods improve as $|d|$ increases. However, the transition is much faster with JCR which outperforms other methods and also stabilizes relatively quickly to perfect group assignment; here all JCR variants perform equally well. Results under $p = \{100, 250\}$ give the same picture; see Figures C.1 and C.2 in Appendix C.

Variable selection. For this comparison we initially set a benchmark model which we call the *label-oracle-lasso*. Under this model we assume that the true group labels are known and we perform separate lasso regressions (for each group) based on the default cross-validation options (for tuning the penalty) in package `glmnet`. We further consider a simple *cluster-lasso* model which involves separate group regressions (again using `glmnet` defaults) based

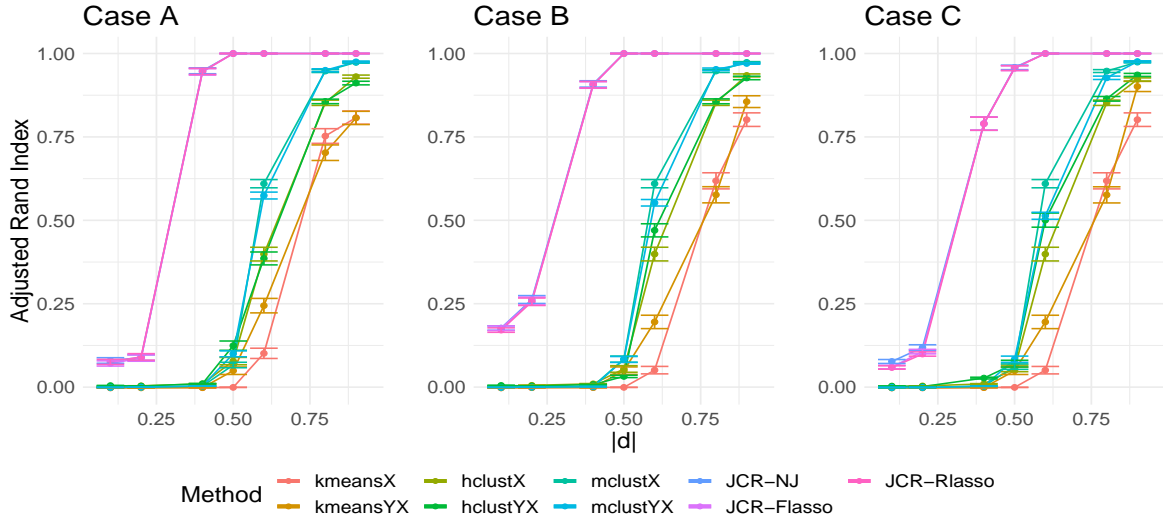


Figure 6: Second simulation, $p = 500$, group assignment. Average adjusted Rand Index (with respect to true group assignments) as a function of the absolute distance ($|d|$) of the group-wise covariate means, for cases A (left), B (center) and C (right). [Results shown over 20 repetitions with error bars indicating standard errors.]

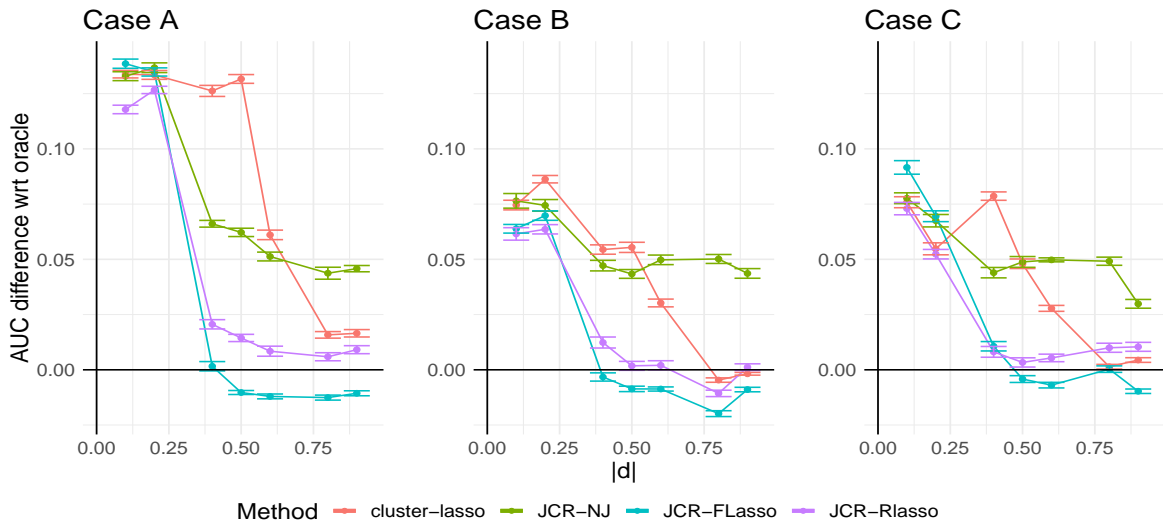


Figure 7: Second simulation, $p = 500$, variable selection. Difference between AUC (in the variable selection sense) between the indicated methods and the oracle-lasso (see text for details) as a function of the absolute distance ($|d|$) of the group-wise covariate means, for cases A (left), B (center) and C (right). [Results shown over 20 repetitions with error bars indicating standard errors.]

on estimated group assignments. Naturally, the cluster-lasso will be almost equivalent to the oracle-lasso model when group assignment is close to perfect. This approach involves an initial clustering step: we give an advantage to the cluster-lasso by using, for each dimension considered, the clustering approach that performs best in a Rand index sense (specifically,

hclust for $p = 100$ and Mclust for $p = \{250, 500\}$).

We summarize results via the area under the ROC curve (AUC) based on the absolute values of the regression coefficients. In particular, we consider the difference between the AUC from oracle-lasso and AUC from competing methods (cluster-lasso and JCR approaches). This provides a measure of regret in terms of AUC from the oracle setting where the true group labels are known. One standard-error plots for the three cases summarized in Table 2 (with $p = 500$) are presented in Figure 7. As expected cluster-lasso yields smaller selection loss (it approaches the oracle-lasso) as the separation of group-wise means increases, but so do the JCR methods. JCR-Flasso is overall better and remarkably tends to result in slightly improved selection in comparison to the oracle-lasso as $|d|$ increases. This is possibly due to the fact that JCR uses weighted estimation based on the entire sample. Furthermore and perhaps most importantly, JCR methods overall outperform the common cluster-lasso approach in low/medium magnitude regions of $|d|$; see also Figures C.3 and C.4 (Appendix C) corresponding to the cases with $p = 100$ and $p = 250$, respectively.

Estimation. We conclude by examining estimation accuracy for the group-wise regression coefficients. Again, comparisons are made with respect to the label-oracle-lasso; this time we consider the increase in root mean squared error (RMSE) resulting from the fact that the group labels are unknown. In this comparison we also consider the *pooled-lasso*; a “naive” model which does not take into account group structure. We include the pooled-lasso in order to investigate the effect of ignoring group structure under each case in Table 2; this is interesting in e.g. case A where the common-location coefficients have opposite signs.

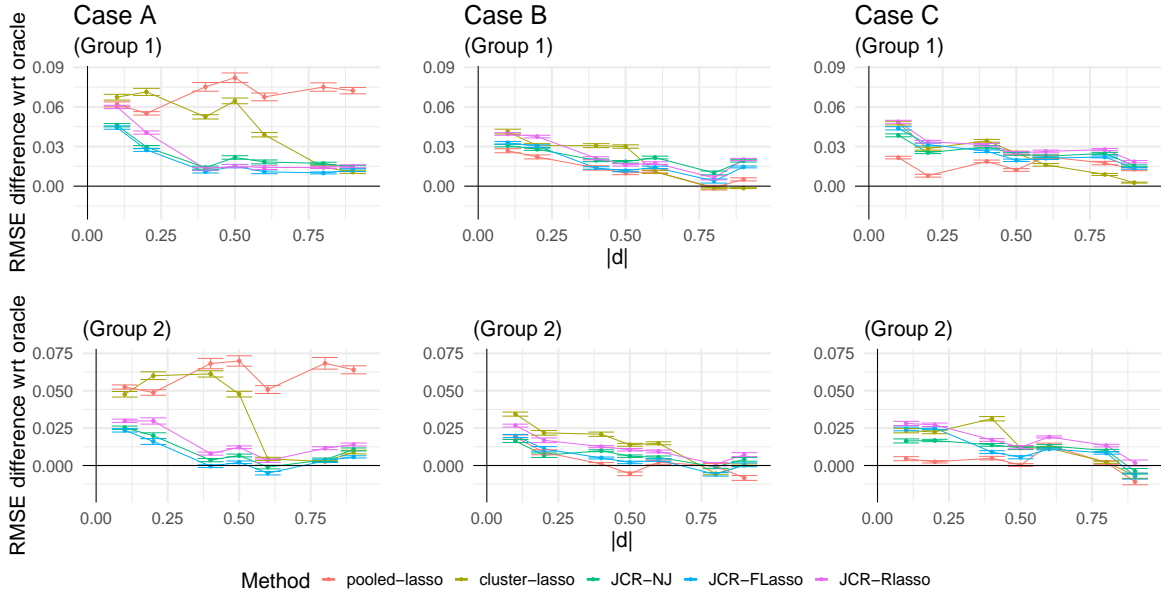


Figure 8: Second simulation, $p = 500$, estimation. Increase in RMSE relative to the oracle-lasso (see text) as a function of the absolute distance ($|d|$) of the group-wise covariate means, under group one (top) and group two (bottom), and for cases A (left), B (center) and C (right). [Results shown over 20 repetitions with error bars indicating standard errors.]

Results for the $n < p$ case ($p = 500$) are summarized in Figure 8. Note that we use

standardized coefficients (divided by $\tilde{\sigma}$ in Table 2) for the calculation of RMSE in order to have a common scale across simulations and cases. As expected, under case A the pooled-lasso model indeed performs poorly. We further see that the JCR methods provide overall better estimates in comparison to the cluster-lasso approach. Under cases B and C, cluster-lasso and JCR methods which are over-parameterized (common-location effects are equal) perform more or less the same and are in general comparable to the pooled-lasso which is under-parameterized (due to the disjoint-location effects). In Appendix C we present the corresponding illustrations for the $n > p$ ($p = 100$, Figure C.5) and $n = p$ ($p = 250$, Figure C.6) cases; results are in general similar with the difference that cluster-lasso performs better when $|d| \approx 1$ and JCR-RLasso performs worse when $|d| \approx 0$. Overall, our illustrations suggest that the JCR-FLasso is the most stable method, followed by JCR-NJ.

6.2.2 Inference for unknown number of groups

We now turn our attention to cluster-selection performance under JCR methods (according to the approach described in Section 5) for model settings where the true number of groups is not given *a priori*. As described in the beginning of Section 6.2 we have data available for four types of cancer; this allows us to consider three simulation settings where the respective true number of groups is $g^* = 2$ (using the BRCA and KIRC cancer types), $g^* = 3$ (BRCA, KIRC, LUAD) and $g^* = 4$ (further including THCA). For each setting we fit JCR models with two, three and four components; i.e. we always consider three competing models. The simulations are along the lines of Section 6.2.1 (same data generating mechanisms), considering case A of Table 2 (which is the most interesting case overall) for $p = 100$. The conditions outlined in Table 2 for the β_j^* 's at the common locations are used again for $g^* \in \{3, 4\}$. Here we use the real group-sample proportions as they occur in the TCGA data set; i.e. we deal with unbalanced designs. In addition, we assume that sample size grows with number of groups in order for the three simulations to be on an equal basis (obviously, if n is fixed cluster selection becomes more difficult as g^* grows). Specifically, we set $n = 250 \times g^*$. The resulting group sample sizes for $g^* \in \{2, 3, 4\}$ are $(n_1 = 335, n_2 = 165)$, $(n_1 = 382, n_2 = 188, n_3 = 180)$ and $(n_1 = 410, n_2 = 200, n_3 = 200, n_4 = 190)$, respectively. Cluster selection based on the estimator in (42) requires, of course, keeping held-out test data. Here, we utilize 80% of the samples for training and 20% for testing.

Figure 9 shows barplots of the selected number of clusters resulting from 50 repetitions of the simulations. As seen, the correct model is selected in majority under all cases and also all JCR methods. The detection rate of the correct model is also annotated in each panel of Figure 9. Here, JCR-NJ is slightly better with average overall detection rate of 59%, while RLasso and FLasso have 56% and 55%, respectively.

7 Discussion

We introduced a class of regularized mixture models that jointly deal with sparse covariance structure and regression modelling in the context of latent groups. Latent group structure is a key concern in modern data-intensive applications, in both applied statistics and machine learning. This is due to the fact that latent structure can strongly confound estimates and lead to practical difficulties if ignored or not properly accounted for but is at the same time inherently difficult to deal with in the multivariate settings typical of modern applications.

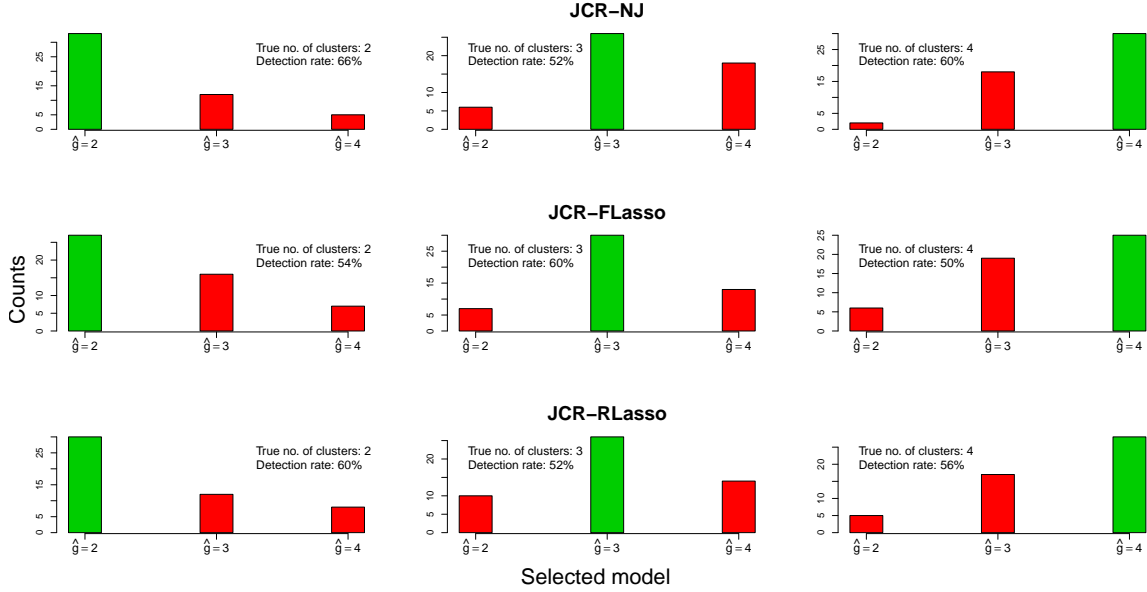


Figure 9: Third simulation, cluster selection. Barplots of selected clusters (under 50 repetitions) from JCR-NJ (top panels), JCR-FLasso (middle panels) and JCR-RLasso (bottom panels). Correct identification is highlighted in green; true number of clusters and detection rate of the correct model is annotated in each panel.

We showed that principled joint modelling of these two aspects leads to gains with respect to simpler decoupled or pooled strategies and that exploiting established ℓ_1 -penalized tools and related Bayesian approaches within the framework we propose leads to practically applicable solutions.

In settings where hidden group structure may be present and where model parameters are intended to have a scientific interpretation we think pooled analysis should be avoided or viewed critically, due to the risk of (potentially severe) confounding by the hidden variable. This setting has interesting connections to current discussions in machine learning on distributional shifts and shift-robust learning; see e.g. [Sinha et al. \(2018\)](#); [Recht et al. \(2018\)](#); [Heinze-Deml and Meinshausen \(2019\)](#). In particular, we think JCR would be a useful tool for shift-robust learning, since it could be used to block paired data (X, Y) into distributionally non-identical groups which could in turn be used to train and test predictors in a shift-robust fashion. This would allow the notion of shift-robust learning to be extended to the case where distributional regimes are not even known at the outset. For pure prediction problems where the test setting is truly global/pooled, the situation is less worrying, since then the standard predictive loss is in a sense acceptable even if the data harbour hidden group structure. In such settings, whether or not potential latent structure should be a concern is an application-specific question.

In this work we utilized the graphical lasso approach for covariance estimation. For the regression coefficients we considered: (i) the Bayesian lasso prior under two strategies (FLasso/RLasso) for setting the penalty parameter, and (ii) the NJ prior. Overall, all three methods performed equally well in terms of cluster allocation. JCR-NJ is an interesting tuning-free approach which can perform well (in terms of estimation and selection) in sparse

settings with strong signal as suggested by the results of Section 6.1. JCR-FLasso resulted in better estimation and selection performance in the semi-synthetic simulations of Section 6.2.1. Our main goal in these comparisons was to explore some of the available regularization options but we note that many other choices would be possible within our framework. JCR is fairly modular in the sense that other methods from the penalized likelihood literature or the Bayesian literature on shrinkage priors – recent reviews provided by Desboulets (2018) and van Erp et al. (2019), respectively – could be used within the same framework.

The proposed framework implemented using the regularized estimation described here is scalable to large- p settings and can also handle the $p > n$ case. However, we did not consider the very high-dimensional setting. Indeed, under the current model specification JCR can become computationally burdensome for very large p , mainly due to the part of the model relating to covariance estimation. However, we think that this can be addressed within our general scheme by combining JCR with ideas from high-dimensional projections. This is an interesting direction for future work. Further future research directions include extensions of the proposed latent model framework to generalized linear models and mixed models for longitudinal data.

References

- Bae, K. and Mallick, B. (2004), ‘Gene selection using a two-level hierarchical Bayesian model’, *Bioinformatics* **20**, 3423–3430.
- Carvalho, C., Polson, N. and Scott, J. (2010), ‘The horseshoe estimator for sparse signal’, *Biometrika* **97**, 465–480.
- Celeux, G., Frühwirth-Schnatter, S. and Robert, C. (2018), Model Selection for Mixture Models – Perspectives and Strategies, In G. Celeux, S. Frühwirth-Schnatter and C. Robert, eds., *Handbook of Mixture Analysis*, Chapter 7, CRC Press.
- Crowley, E. M. (1997), ‘Product partition models for normal means’, *Journal of the American Statistical Association* **92**, 192–198.
- Desboulets, L. D. D. (2018), ‘A review on variable selection in regression analysis’, *Econometrics* **6**(4).
- Donoho, D. L. and Johnstone, J. M. (1994), ‘Ideal spatial adaptation by wavelet shrinkage’, *Biometrika* **81**, 425–455.
- Figueiredo, M. A. T. (2001), ‘Wavelet-based image estimation: An empirical Bayes approach using Jeffreys noninformative prior’, *IEEE Transactions on Image Processing* **10**, 1322–1331.
- Figueiredo, M. A. T. (2003), ‘Adaptive sparseness for supervised learning’, *IEEE Transactions on Pattern Analysis and Machine Intelligence* **25**, 1150–1159.
- Friedman, J., Hastie, T. and Tibshirani, R. (2008), ‘Sparse inverse covariance estimation with the graphical lasso’, *Biostatistics* **9**, 432–441.

- Griffin, J. and Brown, P. (2005), Alternative prior distributions for variable selection with very many more variables than observations, Technical report, University of Warwick.
- Heinze-Deml, C. and Meinshausen, N. (2019), ‘Conditional variance penalties and domain shift robustness’, *arXiv:1710.11469v5 [stat.ML]* .
- Ingrassia, S., Minotti, S. C. and Vittadini, G. (2012), ‘Local statistical modeling via a cluster-weighted approach with elliptical distributions’, *Journal of Classification* **2**, 363–401.
- Khalili, A. and Chen, J. (2007), ‘Variables selection in finite mixture of regression models’, *Journal of the American Statistical Association* **102**, 1025–1038.
- Liverani, S., Hastie, D. I., Azizi, L., Papathomas, M. and Richardson, S. (2015), ‘PREMiuM: An R package for profile regression mixture models using Dirichlet processes’, *Journal of Statistical Software* **64**.
- McLachlan, G. and Peel, D. (2000), *Finite Mixture Models*, John Wiley, New York, USA.
- Meinshausen, N. and Bühlmann, P. (2006), ‘High-dimensional graphs and variable selection with the lasso’, *The Annals of Statistics* **34**, 1436–1462.
- Meng, X.-L. and Rubin, D. B. (1993), ‘Maximum likelihood estimation via the ECM algorithm: A general framework’, *Biometrika* **80**, 267–278.
- Müller, P., Quintana, F. and Rosner, G. L. (2011), ‘A product partition model with regression on covariates’, *Journal of Computational and Graphical Statistics* **20**, 260–278.
- Molitor, J., Papathomas, M., Jerrett, M. and Richardson, S. (2010), ‘Bayesian profile regression with an application to the National survey of childrens health’, *Biostatistics* **11**, 484–498.
- Park, T. and Casella, G. (2008), ‘The Bayesian lasso’, *Journal of the American Statistical Association* **103**, 681–686.
- Pearl, J., Glymour, M. and Jewell, N. (2016), *Causal Inference in Statistics: A Primer*, John Wiley, New York, USA.
- Polson, N. G. and Scott, J. G. (2010), Shrink Globally, Act Locally: Sparse Bayesian Regularization and Prediction, In J.M. Bernardo, M.J. Bayarri, J.O. Berger, A.P. David, D. Heckerman, A.F.M. Smith and M. West, eds., *Bayesian Statistics*, Vol. 9, Oxford University Press, pp. 501–538.
- Recht, B., Roelofs, R., Schmidt, L. and Shankar, V. (2018), ‘Do CIFAR-10 classifiers generalize to CIFAR-10?’, *arXiv:1806.00451 [cs.LG]* .
- Sinha, A., Namkoong, H. and Duchi, J. (2018), Certifiable distributional robustness with principled adversarial training, 6th International Conference on Learning Representations.
- Städler, N., Bühlmann, P. and van de Geer, S. (2010), ‘ ℓ_1 -penalization for mixture regression models’, *Test* **19**, 209–256.

- Städler, N. and Mukherjee, S. (2013), ‘Penalized estimation in high-dimensional hidden Markov models with state-specific graphical models’, *The Annals of Applied Statistics* **7**, 2157–2179.
- Sustik, M. A. and Calderhead, B. (2012), GLASSOFAST: An efficient GLASSO implementation, Technical Report TR-12-29:1-3, UTCS.
- Taschler, B., Dondelinger, F. and Mukherjee, S. (2019), ‘Model-based clustering in very high dimensions via adaptive projections’, *arXiv:1902.08472v1 [stat.ML]* .
- Tibshirani, R. (1996), ‘Regression shrinkage and selection via the lasso’, *Journal of the Royal Statistical Society B* **58**, 267–288.
- van Erp, S., Oberski, D. L. and Mulder, J. (2019), ‘Shrinkage priors for Bayesian penalized regression’, *Journal of Mathematical Psychology* **89**, 31–50.
- Wang, H. (2012), ‘Bayesian graphical lasso models and efficient posterior computation’, *Bayesian Analysis* **7**, 867–886.
- Yuan, M. and Lin, Y. (2007), ‘Model selection and estimation in the Gaussian graphical model’, *Biometrika* **94**, 19–35.

Appendices

A Objective function under the NJ prior

The hierarchical form of the NJ prior is $\beta_k | \mathbf{S}_k \sim N_p(\mathbf{0}, \mathbf{S}_k)$, where $\mathbf{S}_k = \text{diag}(s_{k1}, \dots, s_{kp})$ assuming *latent* s_{kj} with $\pi(s_{kj}) \propto s_{kj}^{-1}$ for $k = 1, \dots, K$ and $j = 1, \dots, p$. The conditional distribution of any s (dropping momentarily subscripts k, j for simplicity) is

$$p(s|\beta) = \frac{q(s)}{\int q(s)ds}, \text{ with } q(s) = p(\beta|s)s^{-1} \text{ and } \int q(s)ds = |\beta|^{-1}.$$

Given this, it follows that

$$\mathbb{E}_{s|\beta}[s^{-1}] = \int s^{-1}p(s|\beta)ds = \beta^{-2} \quad (\text{A.1})$$

This result will be needed in the derivation of the E-step below. The joint prior of β_k and σ_k^2 is $p(\beta, \sigma^2 | \mathbf{S}) = p(\beta | \mathbf{S})p(\sigma^2) \propto \prod_{k=1}^K \exp\left(-\frac{1}{2}\beta_k^T \mathbf{S}_k^{-1} \beta_k\right) \frac{1}{\sigma_k^2}$. The objective under the NJ prior presented in Eq. (25) in the main paper, is derived as follows.

$$\begin{aligned} Q_{\text{NJ}}^Y(\theta^Y | \theta^{Y(t)}) &= \mathbb{E}_{\mathbf{z}, \mathbf{S} | \mathbf{y}, \mathbf{X}, \theta^{Y(t)}} \left[\log f(\mathbf{y} | \mathbf{X}, \mathbf{z}, \alpha, \beta, \sigma^2) + \log \pi(\beta | \mathbf{S}) + \log \pi(\sigma^2) \right] \\ &= \mathbb{E}_{\mathbf{z} | \mathbf{y}, \mathbf{X}, \theta^{Y(t)}} \left[\log f(\mathbf{y} | \mathbf{X}, \mathbf{z}, \alpha, \beta, \sigma^2) \right] + \mathbb{E}_{\mathbf{S} | \beta^{(t)}} \left[\log \pi(\beta | \mathbf{S}) \right] + \log \pi(\sigma^2) \\ &= \sum_i \mathbb{E}_{\mathbf{z} | \mathbf{y}, \mathbf{X}, \theta^{Y(t)}} \left[\log f(y_i | \mathbf{x}_i, z_i, \alpha, \beta, \sigma^2) \right] + \mathbb{E}_{\mathbf{S} | \beta^{(t)}} \left[\log \pi(\beta | \mathbf{S}) \right] + \log \pi(\sigma^2) \\ &= \sum_{i=1}^n \sum_{k=1}^K m_{ki}^{(t)} \left\{ -\frac{1}{2\sigma_k^2} (y_i - \alpha_k - \mathbf{x}_i^T \beta_k)^2 - \frac{1}{2} \log \sigma_k^2 \right\} \end{aligned} \quad (\text{A.2})$$

$$\begin{aligned} &+ \sum_{k=1}^K \left\{ \mathbb{E}_{\mathbf{S}_k | \beta_k^{(t)}} \left[-\frac{1}{2} \beta_k^T \mathbf{S}_k^{-1} \beta_k \right] \right\} - \sum_{k=1}^K \left\{ \log \sigma_k^2 \right\} \\ &= \sum_{k=1}^K \left\{ -\frac{1}{2\sigma_k^2} (\mathbf{y} - \alpha_k \mathbf{1}_n - \mathbf{X} \beta_k)^T \mathbf{M}_k^{(t)} (\mathbf{y} - \alpha_k \mathbf{1}_n - \mathbf{X} \beta_k) - \frac{n_k^{(t)}}{2} \log \sigma_k^2 \right\} \\ &+ \sum_{k=1}^K \left\{ -\frac{1}{2} \beta_k^T \mathbb{E}_{\mathbf{S}_k | \beta_k^{(t)}} [\mathbf{S}_k^{-1}] \beta_k \right\} - \sum_{k=1}^K \left\{ \log \sigma_k^2 \right\} \end{aligned} \quad (\text{A.3})$$

$$\begin{aligned} &= \sum_{k=1}^K \left\{ -\frac{1}{2\sigma_k^2} (\mathbf{y} - \alpha_k \mathbf{1}_n - \mathbf{X} \beta_k)^T \mathbf{M}_k^{(t)} (\mathbf{y} - \alpha_k \mathbf{1}_n - \mathbf{X} \beta_k) - \frac{n_k^{(t)} + 2}{2} \log \sigma_k^2 \right\} \\ &+ \sum_{k=1}^K \left\{ -\frac{1}{2} \beta_k^T \mathbf{V}_k^{(t)} \beta_k \right\} \end{aligned} \quad (\text{A.4})$$

$$\begin{aligned} &= -\frac{1}{2} \sum_{k=1}^K \left\{ \frac{(\mathbf{y} - \alpha_k \mathbf{1}_n - \mathbf{X} \beta_k)^T \mathbf{M}_k^{(t)} (\mathbf{y} - \alpha_k \mathbf{1}_n - \mathbf{X} \beta_k)}{\sigma_k^2} + \beta_k^T \mathbf{V}_k^{(t)} \beta_k \right. \\ &\quad \left. + (n_k^{(t)} + 2) \log \sigma_k^2 \right\}, \end{aligned}$$

where $m_{ki}^{(t)}$ appearing in (A.2) is given Eq. (17) in the main paper, $\mathbf{M}_k^{(t)} = \text{diag}(\mathbf{m}_k^{(t)})$ with $\mathbf{m}_k^{(t)} = (m_{k1}^{(t)}, \dots, m_{kn}^{(t)})^T$ and $\mathbf{V}_k^{(t)} = \text{diag}(1/\beta_{k1}^{2(t)}, \dots, 1/\beta_{kp}^{2(t)})$. The transition from (A.3) to (A.4) is due to (A.1).

B Further results from Section 6.1

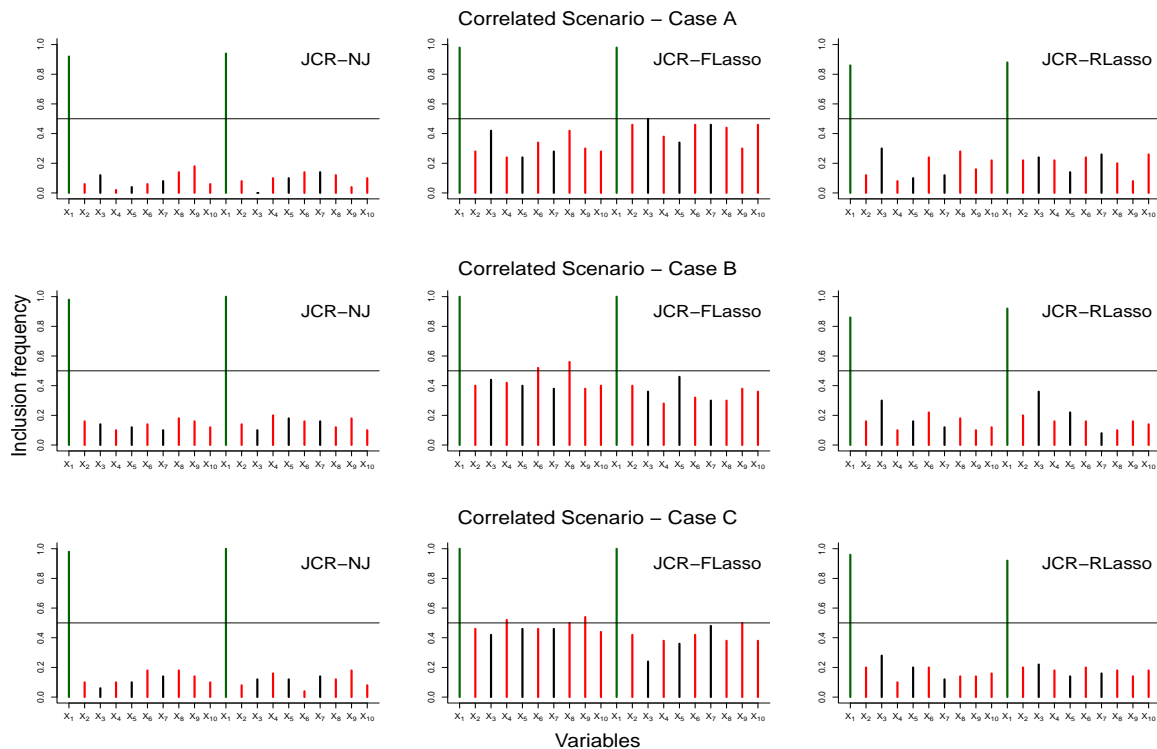


Figure B.1: First simulation, correlated scenario. Variable inclusion frequencies (under 50 repetitions) for signal variables (in green), correlated noise variables (in black) and uncorrelated noise variables (in red) for regression cases A, B and C. Horizontal black lines correspond to a frequency of 0.5.

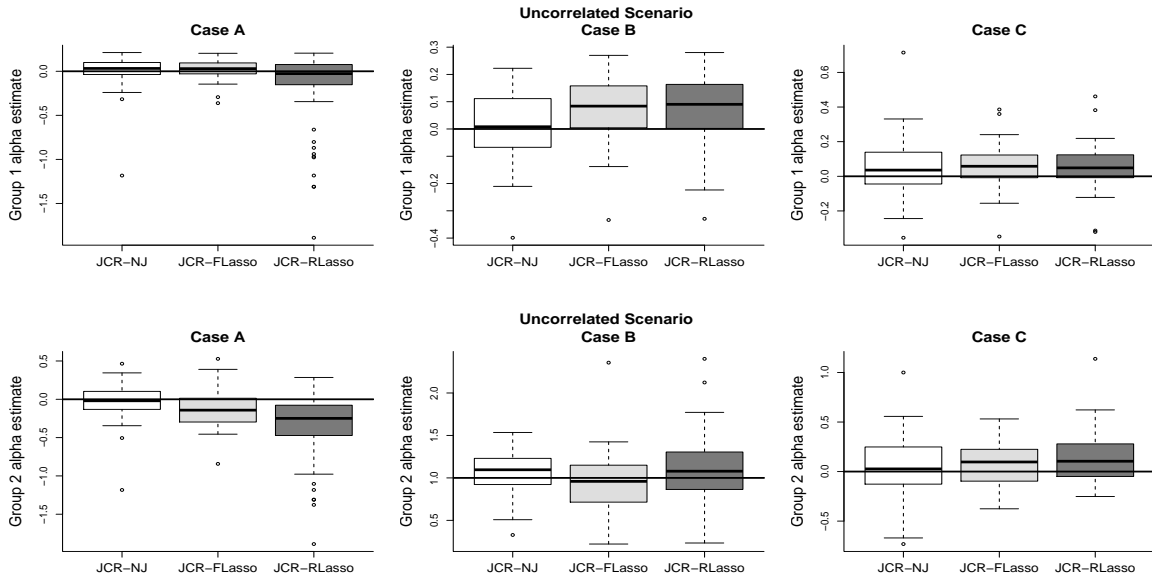


Figure B.2: First simulation, uncorrelated scenario. Boxplots of intercept estimates (from 50 repetitions) of all JCR methods for regression cases A, B and C. Horizontal black lines correspond to the real intercepts.

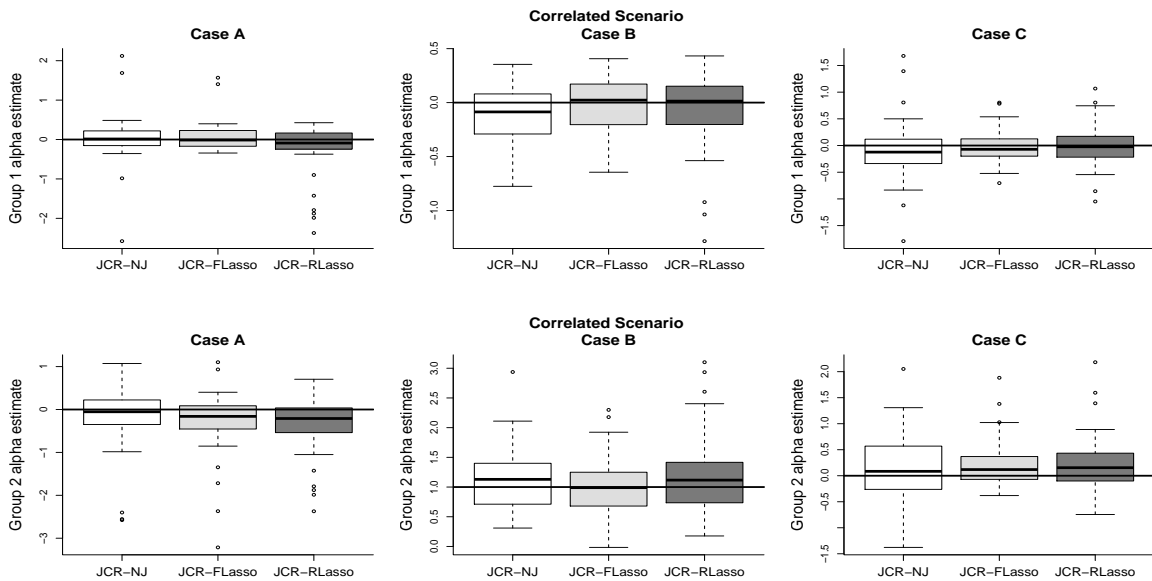


Figure B.3: First simulation, correlated scenario. Boxplots of intercept estimates (from 50 repetitions) of all JCR methods for regression cases A, B and C. Horizontal black lines correspond to the real intercepts.

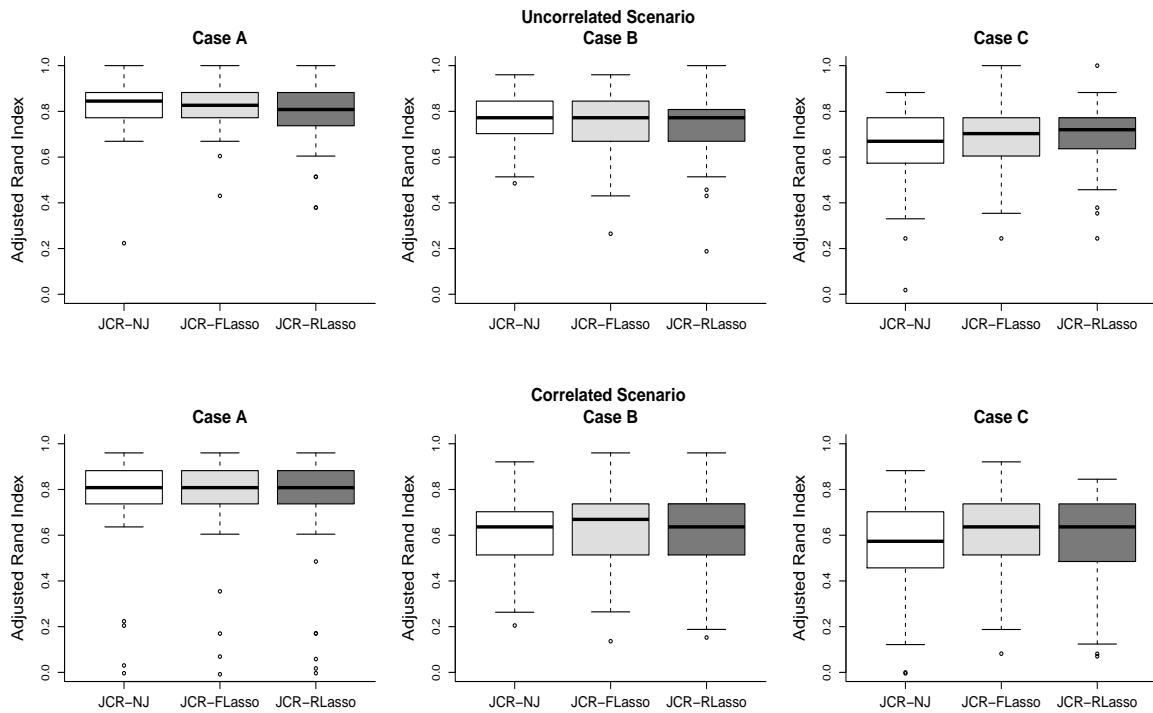


Figure B.4: First simulation. Boxplots of adjusted Rand indexes (from 50 repetitions) of all JCR methods for regression cases A, B and C under the uncorrelated (top panels) and correlated (bottom panels) scenarios.

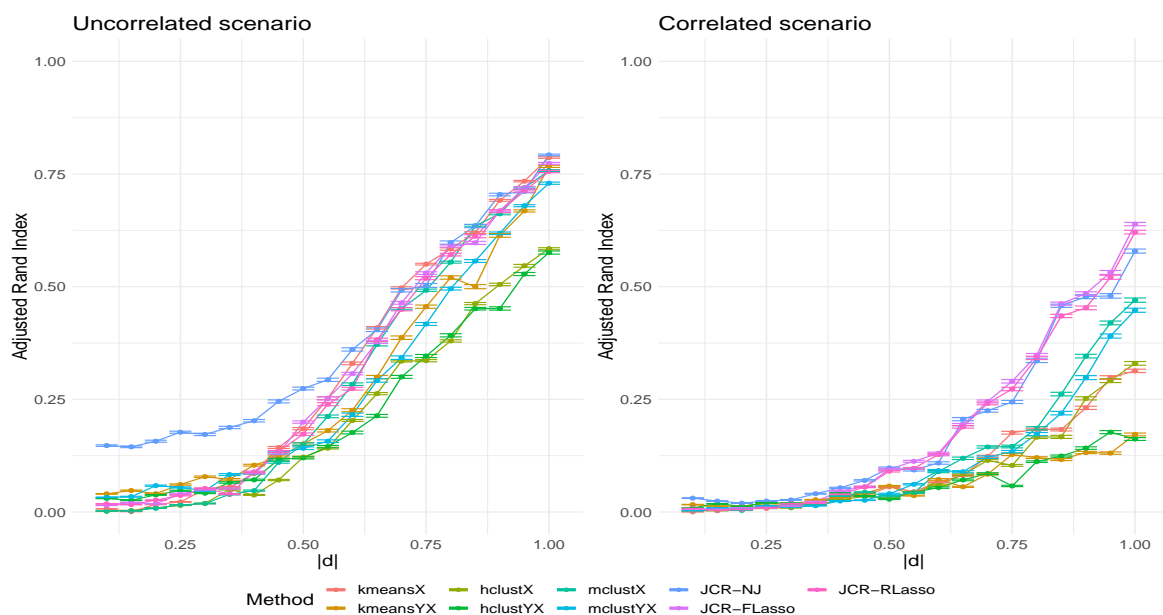


Figure B.5: First simulation, case B. One standard-error bars of adjusted Rand index averages (from 50 repetitions) evaluated over a grid of the absolute distance ($|d|$) of the group-wise covariate means under the uncorrelated scenario (left) and correlated scenario (right).

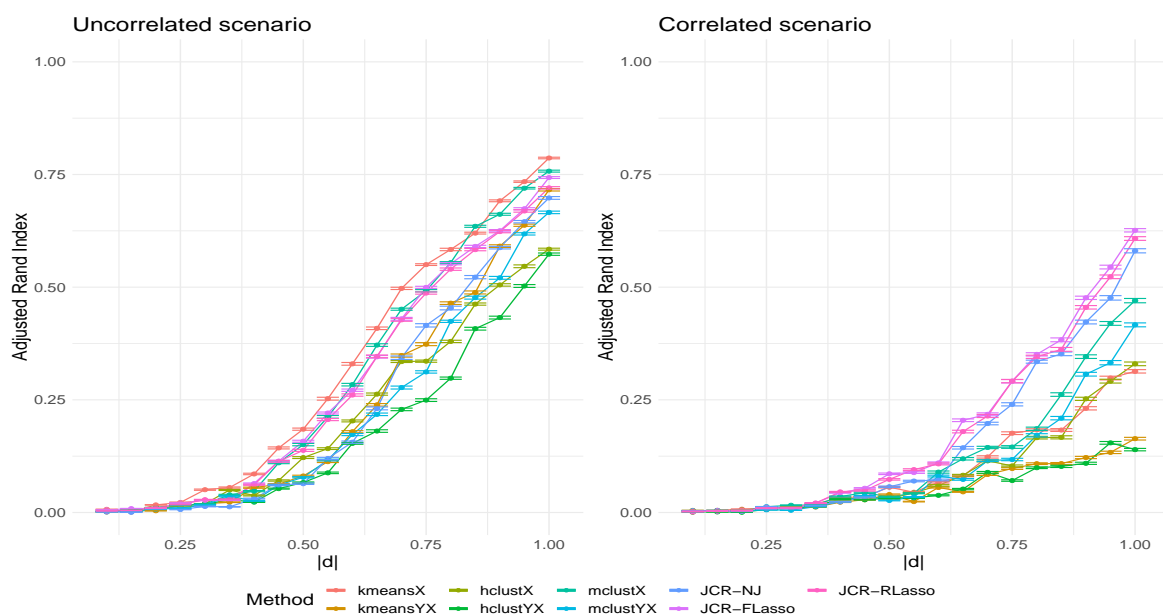


Figure B.6: First simulation, case C. One standard-error bars of adjusted Rand index averages (from 50 repetitions) evaluated over a grid of the absolute distance ($|d|$) of the group-wise covariate means under the uncorrelated scenario (left) and correlated scenario (right).

C Further results from Section 6.2.1

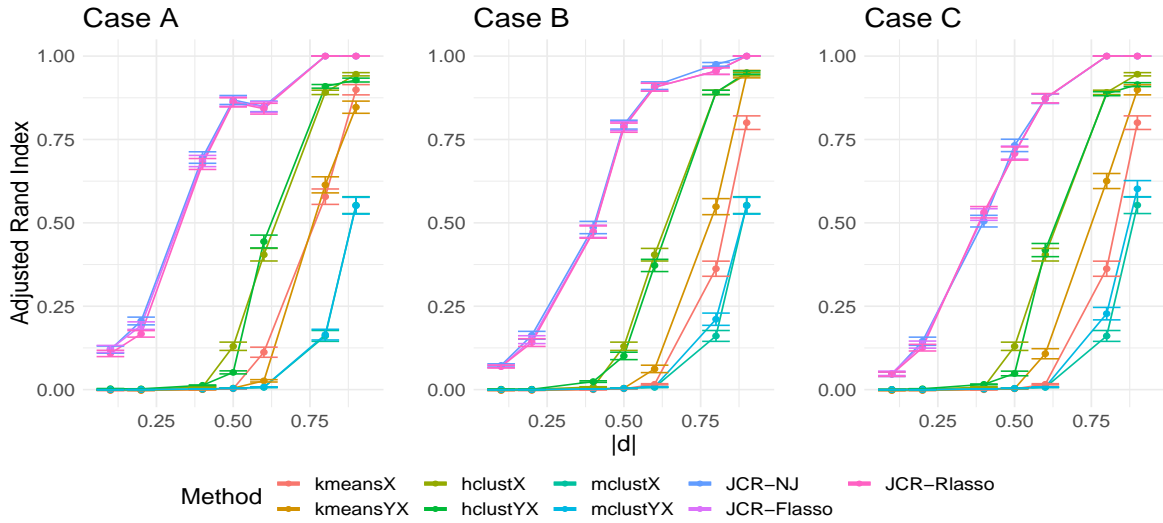


Figure C.1: Second simulation, $p = 100$, group assignment. One standard-error bars of adjusted Rand index averages (from 20 repetitions) evaluated over a grid of the absolute distance ($|d|$) of the group-wise covariate means, for cases A, B and C.

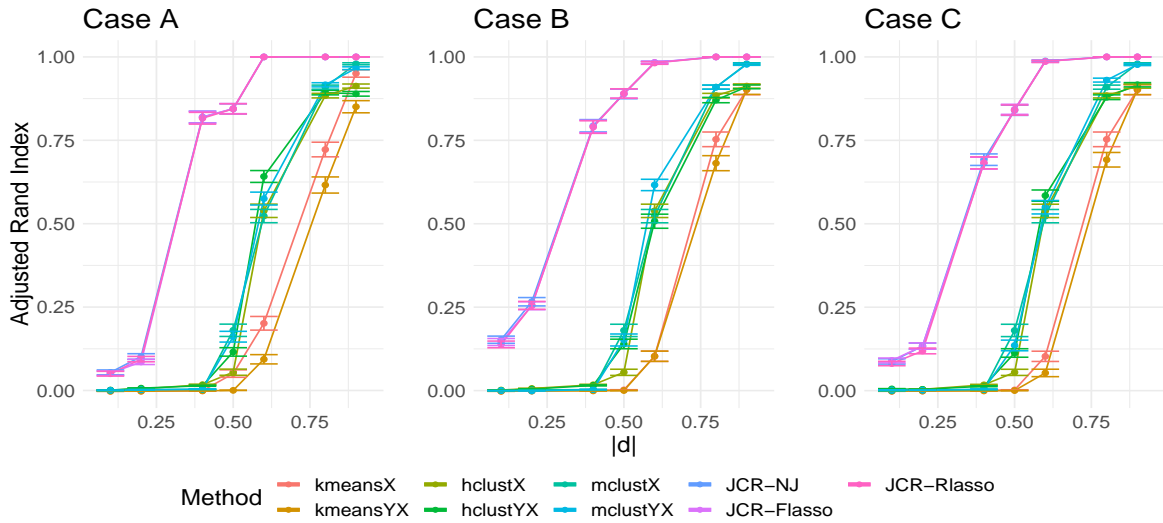


Figure C.2: Second simulation, $p = 250$, group assignment. One standard-error bars of adjusted Rand index averages (from 20 repetitions) evaluated over a grid of the absolute distance ($|d|$) of the group-wise covariate means, for cases A, B and C.

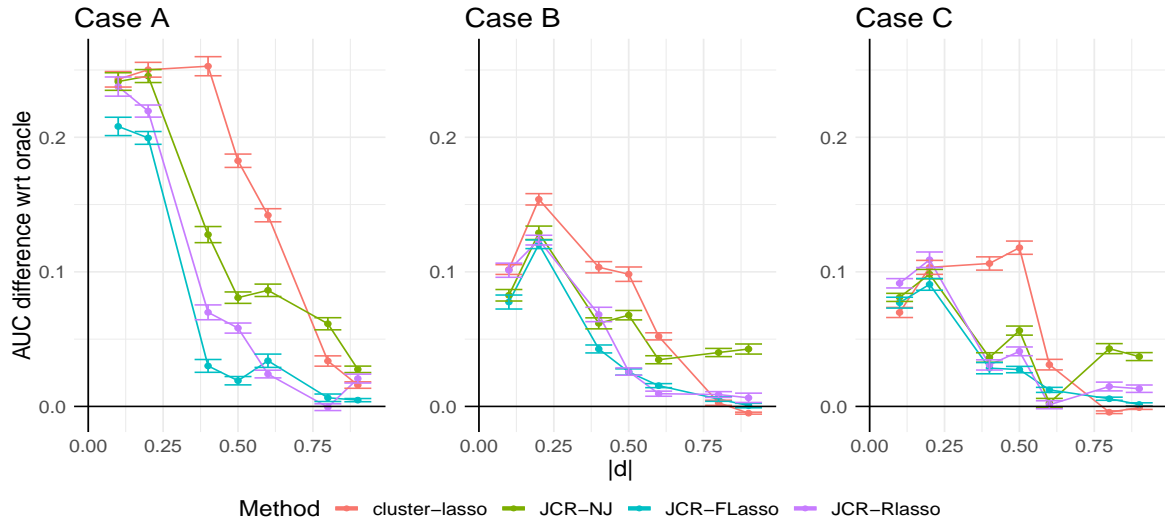


Figure C.3: Second simulation, $p = 100$, variable selection. One standard-error bars of AUC loss-from-oracle averages (from 20 repetitions) evaluated over a grid of the absolute distance ($|d|$) of the group-wise covariate means, for cases A, B and C.

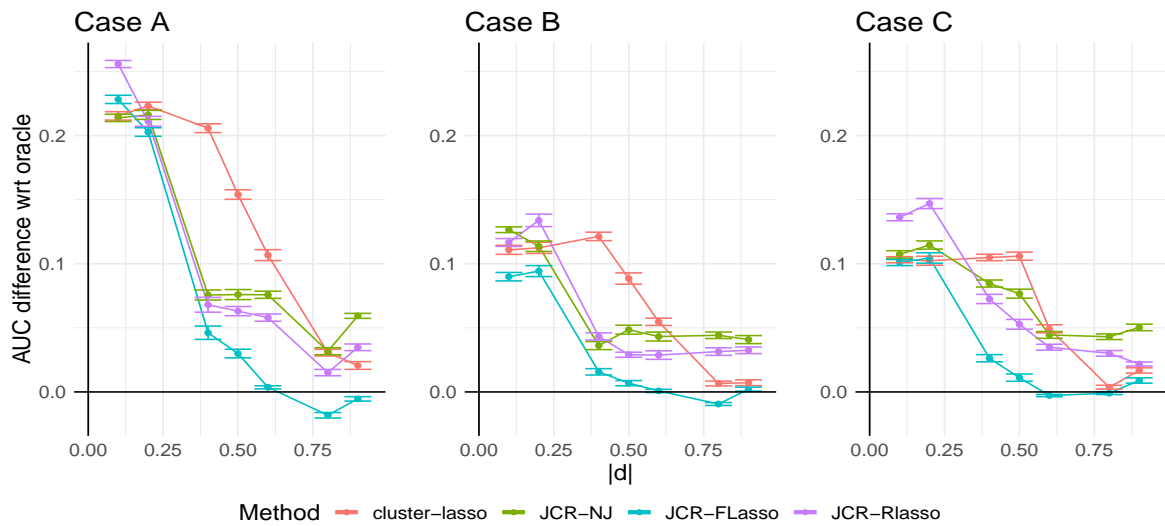


Figure C.4: Second simulation, $p = 250$, variable selection. One standard-error bars of AUC loss-from-oracle averages (from 20 repetitions) evaluated over a grid of the absolute distance ($|d|$) of the group-wise covariate means, for cases A, B and C.

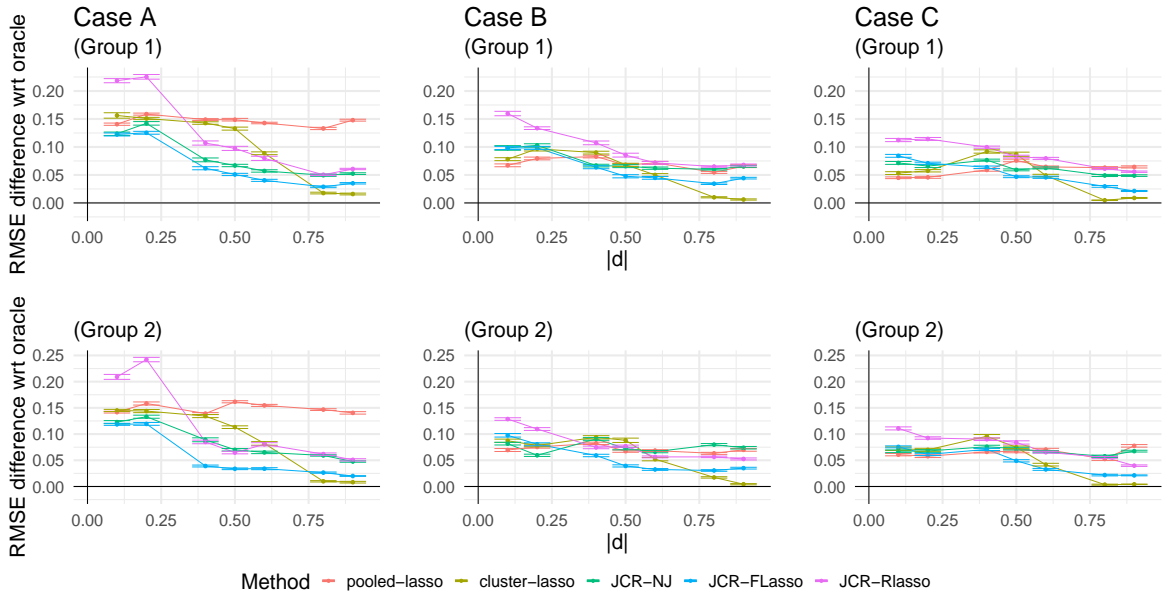


Figure C.5: Second simulation, $p = 100$, regression coefficients estimation. One standard-error bars of RMSE increase-from-oracle averages (from 20 repetitions) evaluated over a grid of the absolute distance ($|d|$) of the group-wise covariate means, under group one (top) and group two (bottom), and for cases A, B and C.

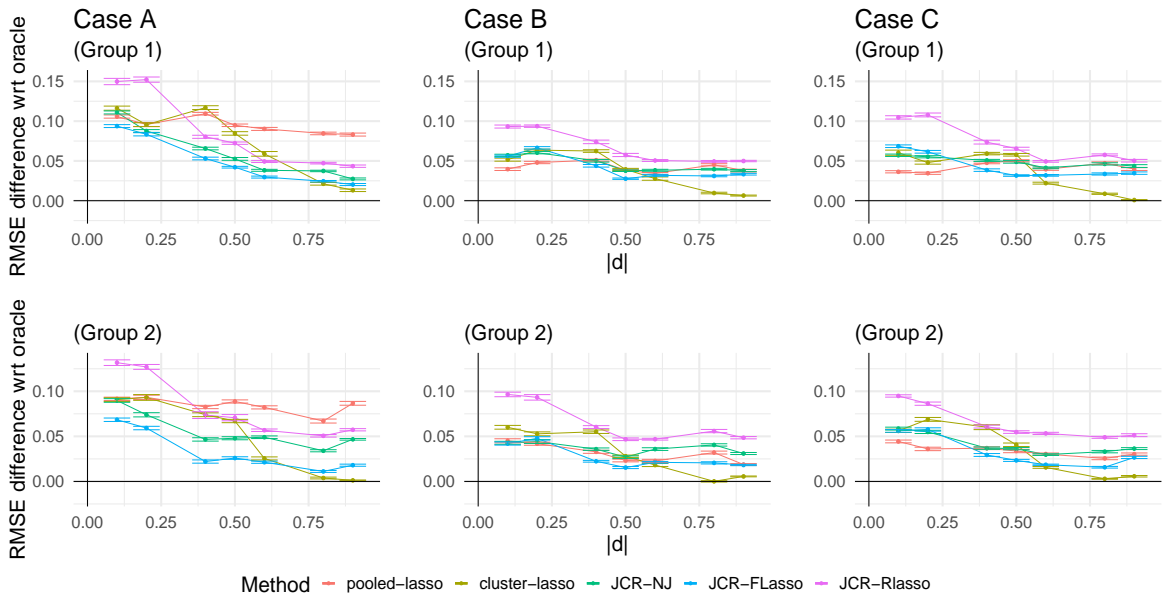


Figure C.6: Second simulation, $p = 250$, regression coefficients estimation. One standard-error bars of RMSE increase-from-oracle averages (from 20 repetitions) evaluated over a grid of the absolute distance ($|d|$) of the group-wise covariate means, under group one (top) and group two (bottom), and for cases A, B and C.